nature plants

Article

https://doi.org/10.1038/s41477-023-01475-0

The SOD7/DPA4–GIF1 module coordinates organ growth and iron uptake in *Arabidopsis*

Received: 30 September 2022

Accepted: 3 July 2023

Published online: 07 August 2023

Check for updates

Leiying Zheng[1,5], Huilan Wu[2,5], Anbin Wang[2,3,5], Yueying Zhang[2,3], Zupei Liu[2,3], Hong-Qing Ling[2,3,4] ✉, Xian-Jun Song[1,3] ✉ & Yunhai Li[2,3] ✉

Organ growth is controlled by both intrinsic genetic factors and external environmental signals. However, the molecular mechanisms that coordinate plant organ growth and nutrient supply remain largely unknown. We have previously reported that the B3 domain transcriptional repressor SOD7 (NGAL2) and its closest homologue DPA4 (NGAL3) act redundantly to limit organ and seed growth in *Arabidopsis*. Here we report that SOD7 represses the interaction between the transcriptional coactivator GRF-INTERACTING FACTOR 1 (GIF1) and growth-regulating factors (GRFs) by competitively interacting with GIF1, thereby limiting organ and seed growth. We further reveal that GIF1 physically interacts with FER-LIKE IRON DEFICIENCY-INDUCED TRANSCRIPTION FACTOR (FIT), which acts as a central regulator of iron uptake and homeostasis. SOD7 can competitively repress the interaction of GIF1 with FIT to influence iron uptake and responses. The *sod7-2 dpa4-3* mutant enhances the expression of genes involved in iron uptake and displays high iron accumulation. Genetic analyses support that *GIF1* functions downstream of *SOD7* to regulate organ and seed growth as well as iron uptake and responses. Thus, our findings define a previously unrecognized mechanism that the SOD7/DPA4–GIF1 module coordinates organ growth and iron uptake by targeting key regulators of growth and iron uptake.

In nature, it is fascinating to see the different organ and seed sizes of plants. Plant organs have to grow to a certain size for optimal functionality[1]. The final size of plant organs is determined by both intrinsic genetic factors and external environmental signals[2–5]. Plant organ growth is coordinately controlled by cell proliferation (increased cell number) and cell expansion (increased cell size)[6–9]. Elucidating genetic and molecular mechanisms underlying organ size control will not only help to understand fundamental developmental processes, but also help to improve crop yield because organ and seed sizes are important yield traits[10,11]. Plants rely on sufficient nutrients to finish their life cycle and produce offspring. However, how plants integrate intrinsic growth signals and external environmental cues to control organ growth is still largely unknown.

Transcriptional regulation is important for plant organ growth and development. The *Arabidopsis* B3 transcription factor superfamily is a plant-specific transcription factor family, encompassing LAV, RAV, ARF and REM families[12]. The RAV family has 13 members, of which *NGATHA* genes (*NGA1–4*), *ABS2* (also known as *NGAL1*), *SOD7* (*NGAL2*) and *DPA4* (*NGAL3*) contain only the B3 domain, while the other 6 members contain the B3 domain and an extra AP2 domain[13,14]. Recently, four *NGATHA* genes in the RAV family have been reported to play key roles in leaf and flower development in *Arabidopsis*. Quadruple *nga* mutants produce big leaves and flowers and show defects in gynoecium development, whereas their respective single mutants have no obvious defects in plant growth, indicating the existence of redundant function among

[1]Key Laboratory of Plant Molecular Physiology, Institute of Botany, Chinese Academy of Sciences, Beijing, China. [2]State Key Laboratory of Plant Cell and Chromosome Engineering, Institute of Genetics and Developmental Biology, Chinese Academy of Sciences, Beijing, China. [3]College of Advanced Agricultural Sciences, University of Chinese Academy of Sciences, Beijing, China. [4]Hainan Yazhou Bay Seed Laboratory, Sanya, China. [5]These authors contributed equally: Leiying Zheng, Huilan Wu, Anbin Wang. ✉e-mail: hqling@genetics.ac.cn; songxj@ibcas.ac.cn; yhli@genetics.ac.cn

the family members[15–18]. *NGAL1–3* also play key roles in the regulation of organ and seed growth. Overexpression of *ABS2* (*NGAL1*) leads to small leaves and flowers[19]. *SOD7* (*NGAL2*) acts redundantly with *DPA4* (*NGAL3*) to regulate organ and seed size in *Arabidopsis*[20]. In addition, *NGAL* genes have been recently described to control leaf margin development[21].

A module consisting of microRNA miR396, GRFs and GIFs, miR396–GRF-GIF, has been reported to regulate organ and seed growth in different plant species[22]. GRFs are streptophyte-specific transcription factors and comprise nine family members in *Arabidopsis*[23]. Functional analysis shows that most GRF proteins positively regulate plant growth and cell proliferation, with the exception of GRF8 (ref. 24). In *Arabidopsis*, loss-of *GRF5* function produces slightly narrow leaves due to reduced cell numbers, whereas overexpression of *GRF5* results in large leaves due to increased cell number[25]. Overexpression of *GRF1* and *GRF2* in *Arabidopsis* also results in large leaves and big seeds. By contrast, the triple-mutant *grf1 grf2 grf3* develops small and narrow leaves, although each single mutant looks very similar to the wild type[26]. GRFs interact with GIFs, which comprise three members in *Arabidopsis* (AtGIF1 (or AN3), AtGIF2 and AtGIF3). GIF1–3 are identified as transcriptional co-activators and act redundantly to control organ growth[25,27,28]. The GRF–GIF complex plays critical roles in plant root, leaf, flower and seed development[22,23,29,30]. Like the *grf* mutants, the *Arabidopsis gif1* mutant has smaller leaves, petals and seeds as a result of reduced cell numbers compared with the wild type[27,31]. By contrast, plants with *GIF1* overexpression exhibit large organs and seeds due to increased cell numbers[25,27,28,31,32]. *GRF* genes expression is post-transcriptionally repressed by a conserved microRNA (miR396). miR396 targets seven out of nine *GRF* genes for cleavage and degradation in *Arabidopsis*[33,34]. Consistent with this, plants with *MIR396* overexpression have small organs, while plants expressing an miR396 target mimic (*MIM396*) produce large leaves[35–37]. These studies demonstrate that the miR396–GRF-GIF module plays a key role in the regulation of organ size.

Plant growth relies on sufficient supply of essential mineral nutrients. Fe plays crucial roles in biomass production and plant product quality[38]. Fe can function as cofactor in fundamental plant biological processes, such as photosynthesis, respiration and chlorophyll biosynthesis. Fe can also participate in many other biochemical pathways, such as hormone and secondary metabolism[39,40]. Plants absorbing enough Fe from soil is also important for human health as most people depend on plants for their primary Fe nutrition. However, excess Fe is toxic to plant growth and development because it has a catalytic role in producing reactive oxygen species[41]. Therefore, plants must tightly control Fe homeostasis. Although soils contain abundant Fe, it is hard to absorb for plants because most exists as insoluble ferric (Fe^{III}) oxyhydrates. *Arabidopsis* utilizes a reduction strategy to facilitate Fe uptake, including acidification of the rhizosphere through release of protons by H^+-adenosine triphosphatases to increase Fe solubility, reduction of Fe(III) chelates to Fe(II), and transportation of Fe(II) into root epidermal cells. Several key members in this strategy have been identified, including PLASMA MEMBRANE PROTON ATPASE 2 (AHA2), FERRIC REDUCTASE OXIDASE 2 (FRO2) and IRON TRANSPORTER 1 (IRT1)[42–44]. The basic *Arabidopsis* helix–loop–helix (bHLH) transcription factor FIT is an orthologue of FER, which activates the expression of Fe uptake genes in tomato roots[45,46]. Under Fe-deficient conditions, FIT interacts with subgroup Ib bHLH transcription factors (bHLH38, bHLH39, bHLH100 and bHLH101) to regulate the expression of *FRO2* and *IRT1* in *Arabidopsis*[47,48]. In modern sustainable agriculture, crops not only require a lot of nutrients to complete their life cycle, but also to improve seed yield and quality. However, how plants coordinate organ and seed growth with nutrient availability remains unclear.

We have previously shown that SOD7 is a negative regulator of seed and organ growth, and the double mutant *sod7-2 dap4-3* shows large seeds and organs[20]. Here we report that SOD7 interacts with GIF1 to coordinate organ growth and Fe uptake in *Arabidopsis*. SOD7 physically interacts with GIF1 and competitively represses the interaction between GIF1 and GRFs, thereby limiting organ and seed growth. SOD7 also inhibits Fe uptake by competitively repressing the interaction between GIF1 and FIT. Genetic analyses support SOD7 functioning antagonistically with GIF1 to control organ growth and Fe uptake. Thus, our findings discover a previously unknown mechanism that the SOD7–GIF1 module coordinates organ growth and Fe uptake.

Results

Interactions between SOD7/DPA4 and GIFs

We previously showed that SOD7 regulates organ and seed size partially by repressing expression of *KLU* in *Arabidopsis*[20]. To further explore the molecular mechanism of SOD7 in organ and seed size control, we screened the SOD7-interacting proteins using the yeast two-hybrid assay. GIF1, a SOD7-interacting protein, was chosen for further analysis because it has been reported to regulate leaf and seed size[27,31]. The interaction between BD-SOD7 and AD-GIF1 was confirmed by co-transforming full-length BD-SOD7 and AD-GIF1 in yeast cells (Fig. 1a). To determine which domains of SOD7 could interact with GIF1, we divided SOD7 into two fragments (an N-terminal fragment SOD7-N with the B3 domain, and a C-terminal fragment SOD7-C) and performed the yeast two-hybrid assay (Fig. 1b). SOD7-C interacted with GIF1, whereas SOD7-N did not (Fig. 1a). Next, a pull-down assay was used to test whether SOD7 could physically interact with GIF1. As shown in Fig. 1c, compared with the negative control MBP protein, the GST–GIF1 fusion protein was able to bind the MBP–SOD7 fusion protein, but not the negative control MBP, indicating that SOD7 physically interacts with GIF1 in vitro. We further investigated the SOD7–GIF1 interaction in planta. A split luciferase complementation assay was used to detect the interaction between SOD7 and GIF1. We coexpressed cLUC–SOD7 (SOD7 fused with the C terminus of luciferase) and GIF1–nLUC (GIF1 fused with N terminus of luciferase) in *Nicotiana benthamiana* leaves. Luciferase signal was observed when GIF1–nLUC and cLUC–SOD7 were coexpressed, whereas the negative control did not show luciferase activity, indicating that SOD7 associates with GIF1 in vivo (Fig. 1d). We then employed a co-immunoprecipitation (Co-IP) assay to verify their interaction in planta. *35S:Myc–SOD7* was transiently coexpressed with either *35S:GFP–GIF1* or *35S:GFP* in *N. benthamiana* leaves. We extracted total proteins and incubated with GFP beads. The immunoprecipitated proteins were then detected by anti-GFP and anti-Myc antibodies. The results revealed that Myc–SOD7 associated with GFP–GIF1, but not with free GFP (Fig. 1e). Thus, these results demonstrated that SOD7 physically interacts with GIF1 both in vitro and in vivo.

Previous studies showed that GIF1 and its homologues GIF2 and GIF3 function redundantly to regulate plant growth and development[27,28,32]. Considering that SOD7 interacted with GIF1, we asked whether SOD7 could also interact with GIF2 and GIF3. We performed a pull-down assay. GIF2 and 3 fused with a GST tag to generate GST–GIF2 and 3, and GST was used as a negative control. As shown in Extended Data Fig. 1a, MBP–SOD7 interacted with GST–GIF2 and GST–GIF3, but not with the negative control GST, indicating that SOD7 can interact with GIF2 and GIF3 in vitro. Next, we employed a split luciferase complementation assay to confirm the interactions between SOD7 and GIF2 and 3. Strong luciferase signals were observed when cLUC–SOD7 and GIF2/3–nLUC were coexpressed, indicating that SOD7 and GIF2 and 3 can interact with each other in vivo (Extended Data Fig. 1b).

We previously revealed that SOD7 works redundantly with its homologue DPA4 to regulate seed and organ size. Because SOD7 associates with GIFs, we asked whether DPA4 could also interact with GIFs. Again, we used a pull-down assay to test the interaction of DPA4 with GIF1–3. As shown in Extended Data Fig. 2a, MBP–DPA4 was pulled down by GST–GIF1–3, but not by GST alone, supporting the hypothesis that DPA4 physically interacts with GIF1, 2 and 3 in vitro. We then coexpressed cLUC–DPA4 and nLUC–GIF1–3 in *N. benthamiana* leaves and analysed their interactions using a split luciferase complementation assay. Strong signals were detected when cLUC–DPA4 and nLUC–GIF1–3 were

https://doi.org/10.1038/s41477-023-01475-0

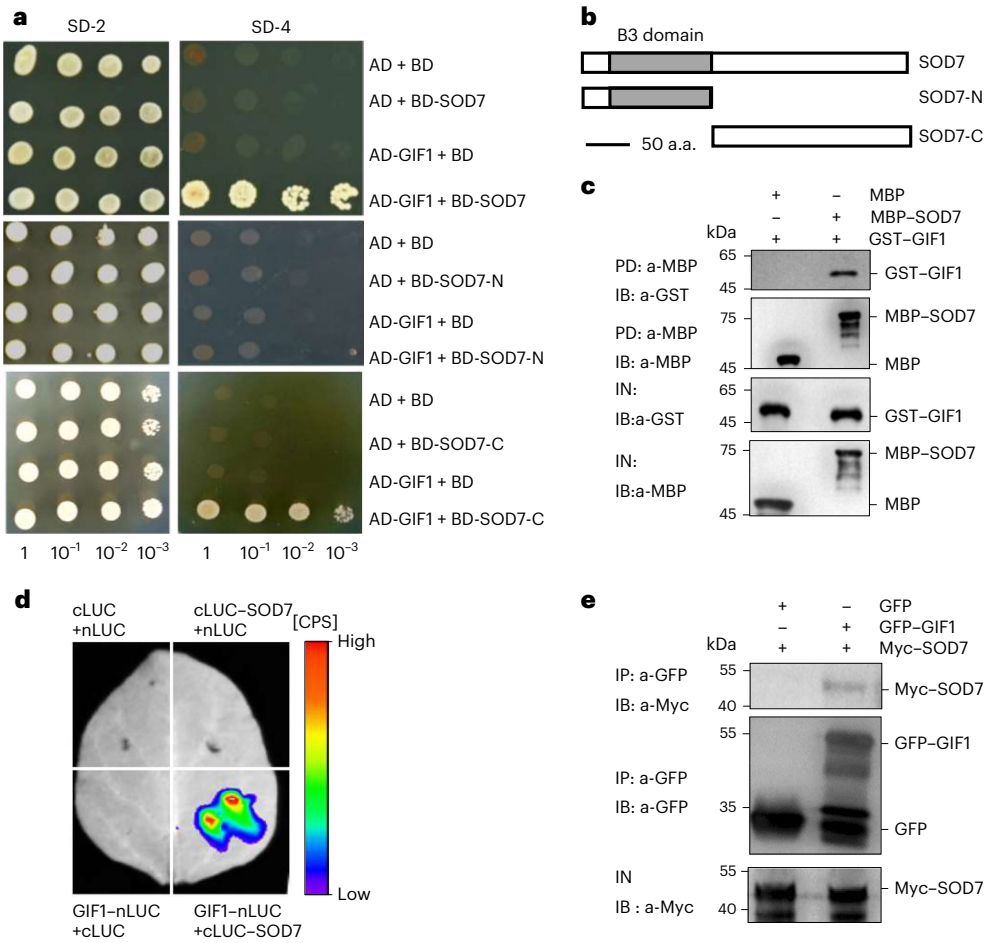

Fig. 1 | SOD7 interacts with GIF1 in vitro and in vivo. a, SOD7 interacts with GIF1 in yeast two-hybrid assays. The construct pairs as indicated were co-transformed into yeast cells. Interactions between bait and prey were tested on the control medium SD-2 (SD without Leu or Trp) and selective medium SD-4 (SD without Ade, His, Leu or Trp). Numbers below the figure represented the dilutions of yeast cells, 1:10, 1:100 and 1:1000. **b**, SOD7 protein structure and fragments used for yeast two-hybrid assay. **c**, SOD7 binds GIF1 in pull-down assays. GST–GIF was pulled down by MBP–SOD7 immobilized on maltose resin and analysed by immunoblotting with an anti-GST or anti-MBP antibody. **d**, The interaction between SOD7 and GIF1 was detected by split luciferase complementation assays. *N. benthamiana* leaves were co-infiltrated with the *Agrobacterium* GV3101 containing different plasmids combinations for 48 h and then images were determined by a CCD camera. The pseudocolour scale bar indicates the range of luminescence intensity. **e**, GIF1 associates with SOD7 in vivo. *35S:myc–SOD7* and *35S:GFP–GIF1* plasmids or *35S:myc–SOD7* and *35S:GFP* only were coexpressed in *N. benthamiana* leaves for 72 h. Total proteins were extracted and immunoprecipitated with GFP–Trap-A and then analysed with anti-Myc and anti-GFP antibodies. IP, immunoprecipitation; IB, immunoblotting; IN, input. Experiments in **c** and **e** were repeated independently at least twice with similar results.

coexpressed, but not in the negative controls (Extended Data Fig. 2b). Together, these results indicate that DPA4 interacts with GIF1–3 both in vitro and in vivo.

SOD7 and *DAP4* function with *GIF1* to control growth

SOD7 has been reported to act redundantly with *DPA4*, its closest family member, to regulate organ and seed size. The *sod7-2 dpa4-3* double mutant forms large leaves, flowers and seeds[20], whereas the *gif1* mutant produces small leaves, flowers and seeds[25,27,31]. We also found that SOD7 physically interacts with GIF1 (Fig. 1a,c–e). Thus, we speculated that they could function antagonistically in a common pathway to control organ and seed size. To test this, we generated a triple-mutant *gif1 sod7-2 dpa4-3* by crossing *gif1* with *sod7-2 dpa4-3* and investigated the organ and seed size phenotypes of the wild type, *sod7-2 dpa4-3*, *gif1* and *gif1 sod7-2 dpa4-3*. The morphology of the *gif1 sod7-2 dpa4-3* triple mutant was similar to that of *gif1* at the seedling stage (Fig. 2b,e). We then measured the size of the sixth mature leaves. As shown in Fig. 2a,f, *sod7-2 dpa4-3* had longer and wider leaves than Col-0 (Columbia-0), whereas *gif1* produced much smaller leaves than Col-0, consistent with previous reports[20,27]. The triple-mutant *gif1 sod7-2 dpa4-3* formed small leaves, like those observed in the single mutant *gif1*, indicating that SOD7 and DPA4 function in a common pathway with GIF1 to control organ size.

As the leaf size is coordinately determined by cell proliferation and cell expansion, we examined the size of palisade cells in the sixth leaves. The average area of palisade cells in *sod7-2 dpa4-3*, *gif1* and *gif1 sod7-2 dpa4-3* was slightly, but not significantly, larger than that in the wild type (Fig. 2g). By contrast, the number of cells in *sod7-2 dpa4-3* leaves was dramatically increased in comparison to that in wild-type leaves, whereas the number of cells in *gif1* and *gif1 sod7-2 dpa4-3* leaves was significantly decreased (Fig. 2g). Importantly, the number of cells in *gif1 sod7-2 dpa4-3* triple-mutant leaves was similar to that in *gif1* leaves (Fig. 2g), indicating that *gif1* is epistatic to *sod7-2 dpa4-3* with respect to leaf cell number.

We next analysed seed size because it is a key trait that affects not only plant fitness but also crop yield. The average area of *gif1 sod7-2 dpa4-3* seeds was significantly smaller than that of *sod7-2 dpa4-3* seeds, indicating that the *gif1* mutation partially suppresses the big

https://doi.org/10.1038/s41477-023-01475-0

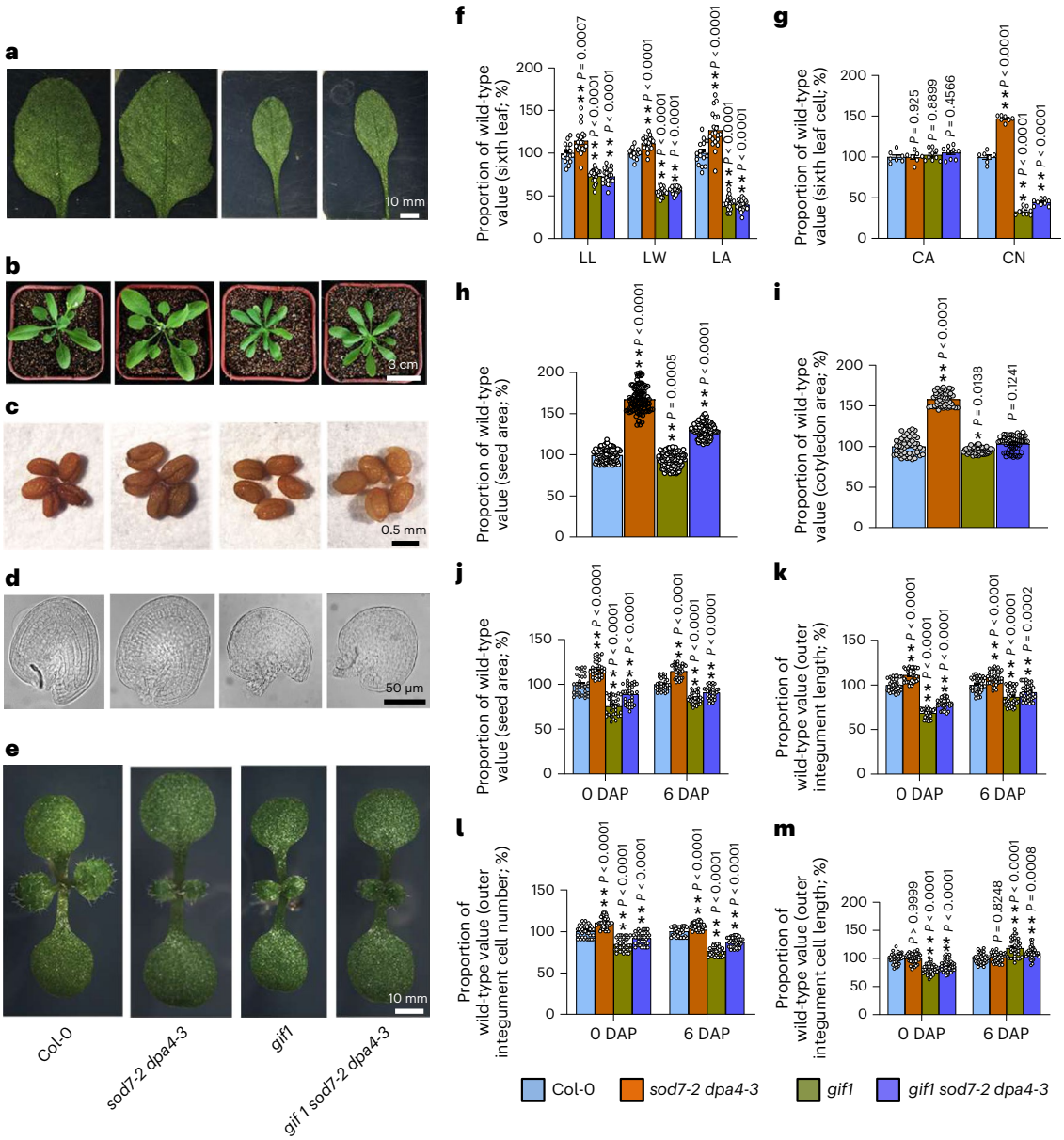

Fig. 2 | *GIF1* genetically works with *SOD7* to control organ and seed size. **a**, The sixth leaf of Col-0, *sod7-2 dpa4-3*, *gif1* and *gif1 sod7-2 dpa4-3* plants. **b**, Twenty-seven DAG plants of Col-0, *sod7-2 dpa4-3*, *gif1* and *gif1 sod7-2 dpa4-3* plants. **c**, Seeds of Col-0, *sod7-2 dpa4-3*, *gif1* and *gif1 sod7-2 dpa4-3* plants. **d**, Ovules of Col-0, *sod7-2 dpa4-3*, *gif1* and *gif1 sod7-2 dpa4-3* plants. **e**, Seven-day-old seedling of Col-0, *sod7-2 dpa4-3*, *gif1* and *gif1 sod7-2 dpa4-3* plants. **f**, The sixth leaf length (LL), width (LW) and area (LA) of Col-0, *sod7-2 dpa4-3*, *gif1*, *gif1 sod7-2 dpa4-3* plants ($n = 15$ leaves for Col-0; $n = 20$ for *sod7-2 dpa4-3*; $n = 22$ for *gif1* and *gif1 sod7-2 dpa4-3*). **g**, The sixth leaf cell area (CA) and cell number (CN) of Col-0, *sod7-2 dpa4-3*, *gif1*, *gif1 sod7-2 dpa4-3* ($n = 7$ leaves for Col-0 and *sod7-2 dpa4-3*, $n = 9$ for *gif1* and *gif1 sod7-2 dpa4-3*). **h**, The seed area of Col-0, *sod7-2 dpa4-3*, *gif1* and *gif1 sod7-2 dpa4-3* ($n = 101$ seeds). **i**, The cotyledon area of Col-0, *sod7-2 dpa4-3*, *gif1* and *gif1 sod7-2 dpa4-3* ($n = 51$ cotyledons). **j**–**m**, The seed area ($n = 32$ seeds; **j**), outer integument length (**k**), outer integument cell number (**l**) and outer integument cell length (**m**) of Col-0, *sod7dpa4*, *gif1* and *gif1 sod7 dpa4* plants at 0 and 6 DAP ($n = 38$ outer integuments for **k**–**m**). The experiments in **f**–**m** were repeated at least twice with similar results. Values in **f**–**m** represent mean ± s.e.m., and respective Col-0 data set as 100%. Asterisks indicates significant difference, $^{*}P < 0.05$ and $^{**}P < 0.01$ compared with wild type (one-way ANOVA with Dunnett's multiple comparisons test).

seed phenotype of *sod7-2 dpa4-3* (Fig. 2c,h). We then examined cotyledon size, which is positively related to seed size[49,50]. As expected, the *gif1 sod7-2 dpa4-3* triple mutant showed smaller cotyledons than the *sod7-2 dpa4-3* double mutant (Fig. 2e,i), indicating that loss of *GIF1* function suppresses the large cotyledon phenotype of *sod7-2 dpa4-3*. These results indicate that *SOD7* and *DPA4* function, at least in part, in a common pathway with *GIF1* to control seed size.

The size of seeds is coordinately determined by maternal and zygotic tissues. Both *SOD7* and *GIF1* function maternally to control seed size[20,31]. To further understand the effect of *SOD7* and *GIF1* on seed development, we investigated the development of outer integuments. Consistent with previous reports[20,31], *sod7-2 dpa4-3* had obviously bigger ovules compared with the wild type (Fig. 2d). By contrast, *gif1* had smaller ovules than the wild type (Fig. 2d). The *gif1 sod7-2 dpa4-3* triple mutant displayed smaller ovules compared with the *sod7-2 dpa4-3* double mutant (Fig. 2d), indicating that the *gif1* mutation partially suppresses the large ovule phenotype of *sod7-2 dpa4-3*. We then measured the outer integument length of mature ovules at 0 days after pollination (DAP). The outer integument length of *gif1 sod7-2 dpa4-3* is shorter than that of *sod7-2 dpa4-3* at 0 DAP (Fig. 2k). In addition, the

outer integument cell number and cell length in *gif1 sod7-2 dpa4-3* were reduced compared with those in *sod7-2 dpa4-3* at 0 DAP (Fig. 2l,m). After fertilization, the *gif1 sod7-2 dpa4-3* triple mutant had smaller seeds and shorter integuments than the double mutant *sod7-2 dpa4-3*, like those observed in the single mutant *gif1* at 6 DAP (Fig. 2j,k). Thus, *gif1* is epistatic to *sod7-2 dpa4-3* with respect to seed area and integument length at 6 DAP. We further counted the number of cells in the outer integuments of *gif1 sod7-2 dpa4-3* at 6 DAP. The number of cells in the outer integuments of *gif1 sod7-2 dpa4-3* was similar to that in the *gif1* single mutant (Fig. 2l). By contrast, the length of outer integument cells in *gif1* and *gif1 sod7-2 dpa4-3* was longer than that in the wild type (Fig. 2m), suggesting a possible compensation mechanism between cell proliferation and cell elongation[27,51,52]. Taken together, these results supported that *SOD7* and *DAP4* act, at least in part, in a common pathway with *GIF1* to regulate organ and seed size.

SOD7 competitively represses GIF1 and GRFs interaction

To further understand how *SOD7* functions with *GIF1* to control organ and seed size, we first checked the expression level of *GIF1* in the *sod7-2 dpa4-3* double mutant and the expression level of *SOD7* in the *gif1* mutant. As shown in Extended Data Fig. 3a,b, the *GIF1* mutation does not affect the expression level of the *SOD7* gene, and the disruption of *SOD7* and *DPA4* does not influence the expression level of the *GIF1* gene. As GIF1 was identified as a coactivator of the GRF transcription factors to regulate plant organ growth, we asked whether *SOD7* is involved in the *GIF–GRF* pathway. *Arabidopsis* has nine *GRF* family members, and expression levels of seven members are downregulated by miR396. We then detected whether expression levels of these seven *GRF* genes could be influenced in *sod7-2 dpa4-3*. As shown in Extended Data Fig. 3c, expression levels of these seven *GRF* genes in *sod7-2 dpa4-3* mutants were similar to those in the wild type, indicating that *SOD7* and *DPA4* do not regulate the expression of *GRF* genes.

The GIF1 protein normally interacts with GRF proteins to form a functional complex to regulate plant growth and development[23]. Considering that SOD7 physically interacts with GIF1, and they act genetically to regulate organ and seed size, we asked whether SOD7 could inhibit the GIF1-GRFs interaction to influence organ and seed growth. To test this possibility, we chose GRF2 and GRF3 as examples and tested whether SOD7 could inhibit the interaction of GIF1 with GRF2 and GRF3. GRF2 and GRF3 were fused with the C terminus of luciferase to generate cLUC–GRF2 and cLUC–GRF3. We then co-transformed GIF1–nLUC with cLUC–GRF2 or cLUC–GRF3 in *N. benthamiana* leaves. The strong luciferase activity was observed when coexpressing nLUC–GIF1 with cLUC–GRF2 or cLUC–GRF3 (Fig. 3a). When the Myc–SOD7 was added as a competitor, luciferase activities were gradually attenuated along with the increased concentrations of Myc–SOD7 (Fig. 3a,b). By contrast, the interactions of GIF1 with GRF2 and GRF3 were not affected by adding different concentrations of GFP (the negative control; Extended Data Fig. 4a, b), indicating that SOD7 represses the interaction between GIF1 and GRFs by competitively interacting with GIF1. We further performed a Co-IP analysis in *N. benthamiana* leaves and confirmed that the interaction between GIF1 and GRF2 was deceased when SOD7 was added (Extended Data Fig. 5). However, when the TCP15 protein (a negative control) was added, the interaction between GIF1 and GRF2 was not affected (Extended Data Fig. 5). We then performed a bimolecular fluorescence complementation (BiFC) assay in *sod7-2 dpa4-3* protoplasts. The GIF1 fused with the N-terminal portions of Venus (nVenus) and GRF2,3 tagged with the C-terminal portion of CFP (cCFP), with different concentrations of Myc–SOD7, as indicated, were co-transformed into *sod7-2 dpa4-3* protoplasts. The results revealed that coexpression of GIF1–nVenus and GRF2,3–cCFP produced strong signals (Extended Data Fig. 6a,b). When 1 × Myc–SOD7 was added, the interaction between GIF1–nVenus and GRF2,3–cCFP was decreased (Extended Data Fig. 6a,b). When 10 × Myc–SOD7 was added, we rarely observed the interaction between GIF1–nVenus and GRF2,3–cCFP (Extended Data Fig. 6a,b). While the 10 × Myc (the negative control) was added, coexpression of GIF1–nVenus and GRF2,3–cCFP produced strong signals (Extended Data Fig. 6a,b), indicating that SOD7 competitively represses the interaction between GIF1 and GRF2,3.

The miR396–GRF module controls seed size

It has been well documented that GRFs play key roles in organ growth[25,27,29]. *35S:*At*GRF1* and *35S:*At*GRF5* have been shown to increase seed size in *Arabidopsis*, and overexpression of Bn*GRF2a* and Br*GRFs* from *Brassica* produced large seeds in *Arabidopsis*[53–55]. Several GRFs in rice have also been reported to positively regulate grain size[56–60]. However, it is unclear whether loss of function of *GRFs* could influence seed size in *Arabidopsis*. Considering the redundancy between family members, we took advantage of the *MiR396a* overexpression lines that repressed seven out of nine *GRFs* expression and *MIM396* overexprssion lines that inactivated *miR396* to investigate their seed size phenotype. We first detected the expression levels of *GRF* genes in *MIM396* and *MiR396a* plants. As reported previously[61], the expression levels of all seven target *GRF* genes in *MiR396a* plants were decreased compared with those in Col-0 (Extended Data Fig. 7). By contrast, expression levels of several *GRF* genes in *MIM396* plants were increased in comparison with those in the Col-0 (Extended Data Fig. 7). We then measured the average area of Col-0, *MiR396a* and *MIM396* seeds. As we expected, *MiR396a* plants had smaller seeds compared with the wild type, indicating that loss of function of *GRFs* decreases seed size (Fig. 3c,e). Consistent with this, *MIM396* plants produced large seeds compared with the wild type (Fig. 3c,e). To further confirm this result, we germinated the seeds of Col-0, *MiR396a* and *MIM396* and observed their cotyledons. The *MiR396a* plants had smaller cotyledons than Col-0, whereas *MIM396* plants showed bigger cotyledons than Col-0 (Fig. 3d,f). Together, these results showed that the miR396–GRF module regulates seed size in *Arabidopsis*.

The SOD7/DPA4–GIF1 module regulates Fe homeostasis

Our results show that *SOD7* and *GIF1* function in a common pathway to regulate organ and seed growth. However, plants require a lot of nutrients to complete their life cycle. Under the same growth conditions, the *sod7-2 dpa4-3* double mutant had bigger organs and seeds than the wild type. We therefore asked whether *sod7-2 dpa4-3* could have better nutrient use efficiency than the wild type. First, we measured the concentrations of essential elements in shoots of seedlings grown vertically on Murashige and Skoog (MS) medium. Interestingly, the Fe, N, Ca and P content in *sod7-2 dpa4-3* were higher than those in Col-0, whereas Zn and K contents in *sod7-2 dpa4-3* were lower than those in Col-0 (Supplementary Table 1). Considering that *GIF1* acts downstream of *SOD7* to regulate organ and seed size, we further measured the element contents in *gif1* and *gif1 sod7-2 dpa4-3*. Surprisingly, both *gif1* and *gif1 sod7-2 dpa4-3* had much lower Fe content than Col-0, indicating that *gif1* suppresses the high Fe accumulation phenotype of *sod7-2 dpa4-3*. By contrast, *gif1* did not suppress other elemental content of *sod7-2 dpa4-3* (Supplementary Table 1). Thus, these results suggested that *GIF1* functions with *SOD7* and *DPA4* in a common pathway to regulate Fe content (Supplementary Table 1).

As an essential micronutrient, Fe is very important for plant growth. To understand how *SOD7*, *DPA4*, and *GIF1* coordinate organ growth and Fe homeostasis, we investigated the Fe-related phenotypes of Col-0, *sod7-2 dpa4-3*, *gif1* and *gif1 sod7-2 dpa4-3*. We grew Col-0, *sod7-2 dpa4-3*, *gif1* and *gif1 sod7-2 dpa4-3* plants vertically on MS medium with or without Fe supply and analysed their phenotypes after 7 d. On normal MS medium, the colour of these mutant leaves looked similar to that of the wild type, although the *sod7-2 dpa4-3* leaves had higher chlorophyll content compared with Col-0 leaves (Fig. 4a,b). However, on Fe-deficient medium, *sod7-2 dpa4-3* exhibited obviously greener leaves than Col-0, whereas Col-0, *gif1* and *gif1 sod7-2 dpa4-3* showed chlorosis leaves (Fig. 4a). Chlorophyll content in *sod7-2 dpa4-3* leaves

https://doi.org/10.1038/s41477-023-01475-0

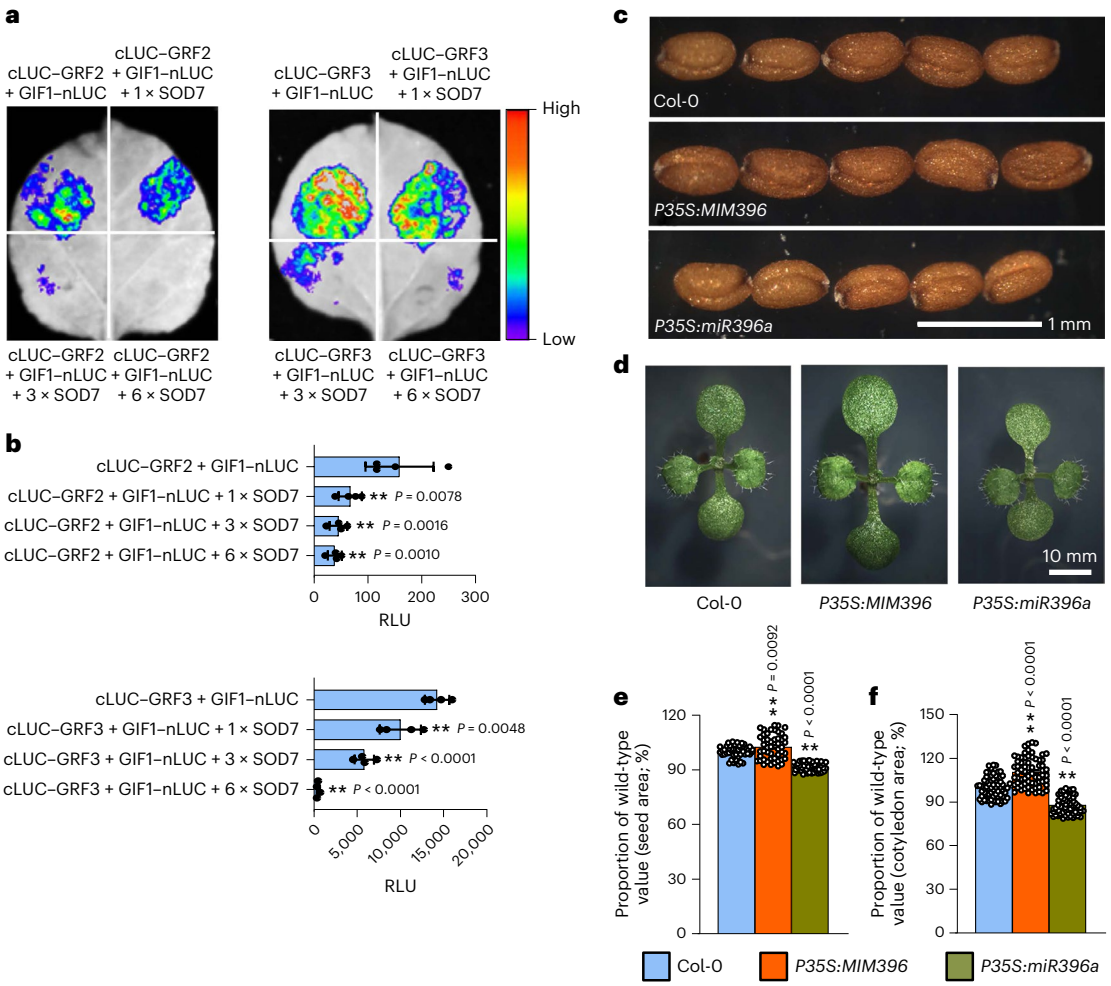

Fig. 3 | SOD7 competes suppressing the interaction between GIF1 and GRFs, and GRFs are involved in seed size control. a, SOD7 competes with the interaction of GIF1 with GRF2 and GRF3, as detected by split luciferase complementation assays. *N. benthamiana* leaves were co-infiltrated with the *Agrobacterium* GV3101 containing combinations as indicated. The pseudocolour scale bar indicates the range of luminescence intensity. **b**, Quantification of LUC signals from **a**. Values represent mean ± s.d. ($n = 4$ biologically independent repeats). **c**, Seeds of Col-0, *P35S:MIM396* and *P35S:miR396a*. **d**, Eight-day-old seedlings of Col-0, *P35S:MIM396* and *P35S:miR396a*. **e**, The seed area of Col-0, *P35S:MIM396* and *P35S:miR396a* ($n = 48$ seeds). **f**, The cotyledon area of Col-0, *P35S:MIM396* and *P35S:miR396a* ($n = 66$ seeds). The experiments in **e** and **f** were repeated independently at least twice with similar results. Values in **e** and **f** represent mean ± s.e.m. and the respective Col-0 data set as 100%. Asterisks indicate significant difference, $^*P < 0.05$ and $^{**}P < 0.01$ compared with no *35S:SOD7* adding samples in **b**, and Col-0 in **e**–**f** (one-way ANOVA with Dunnett's multiple comparisons test). RLU, relative luminescence units.

was significantly higher than in Col-0 leaves, while chlorophyll content in *gif1* leaves was lower than in Col-0 leaves (Fig. 4b). Chlorophyll content in *gif1 sod7-2 dpa4-3* leaves was similar to that in *gif1* leaves (Fig. 4b). These results reveal that the *gif1* mutation is epistatic to *sod7-2 dpa4-3* with respect to leaf colour and chlorophyll content.

We further quantified the root length. Under normal growth conditions, the length of *sod7-2 dpa4-3* roots was similar to that of Col-0 roots, while *gif1* had longer roots than Col-0, consistent with a previous report[29] (Fig. 4c). However, under Fe-deficient conditions, *sod7-2 dpa4-3* exhibited longer roots than Col-0, whereas *gif1* and *gif1 sod7-2 dpa4-3* had shorter roots than Col-0, indicating that the *gif1* mutation suppresses the long root phenotype of *sod7-2 dpa4-3* (Fig. 4c). We then measured Fe content in Col-0, *sod7-2 dpa4-3*, *gif1* and *gif1 sod7-2 dpa4-3* roots, shoots and seeds. Under normal growth conditions, the Fe content in *sod7-2 dpa4-3* roots, shoots and seeds was higher than those in Col-0, whereas the Fe content in *gif1* and *gif1 sod7-2 dpa4-3* shoots and seeds was significantly lower than in Col-0 (Fig. 4d–f). The Fe content in *gif1 sod7-2 dpa4-3* roots, shoots and seeds was similar to *gif1*, indicating that *gif1* is epistatic to *sod7-2 dpa4-3* with respect to the Fe accumulation. Similarly, the *gif1* mutation suppressed the high Fe content phenotype of *sod7-2 dpa4-3* roots and shoots under Fe-deficient conditions (Fig. 4d,e). Consistent with this, the expression of Fe-responsive marker gene At*FER1* (one of four ferritins in *Arabidopsis*), which is tightly regulated by the Fe status in plants and Fe availability in the environment[62,63], was significantly high in *sod7-2 dpa4-3* mutant compared with that in Col-0 (Fig. 4g). By contrast, At*FER1* expression in *gif1* and *gif1 sod7-2 dpa4-3* was dramatically lower than in Col-0 under Fe-deficient conditions (Fig. 4g). The expression level of At*FER1* in *gif1 sod7-2 dpa4-3* was similar to that in *gif1* (Fig. 4g). Together, these results reveal that SOD7 functions antagonistically with GIF1 in a common pathway to regulate Fe responses and accumulation.

Considering that the *sod7-2 dpa4-3* mutant displayed tolerance to Fe-deficiency stress, whereas the *gif1* mutant was sensitive to Fe-deficiency stress, we tested whether the expression of *SOD7* and *GIF1* was regulated by Fe status. As shown in Fig. 4h, expression levels of *SOD7* in Col-0 roots grown on medium with Fe or without Fe were similar. By contrast, the *GIF1* expression was upregulated under Fe-deficient conditions (Fig. 4i). We further analysed protein levels of SOD7 and GIF1. Total proteins were extracted from *proSOD7:SOD7–GFP* and *proGIF1:GIF1–GFP* transgenic plants grown on medium with or

https://doi.org/10.1038/s41477-023-01475-0

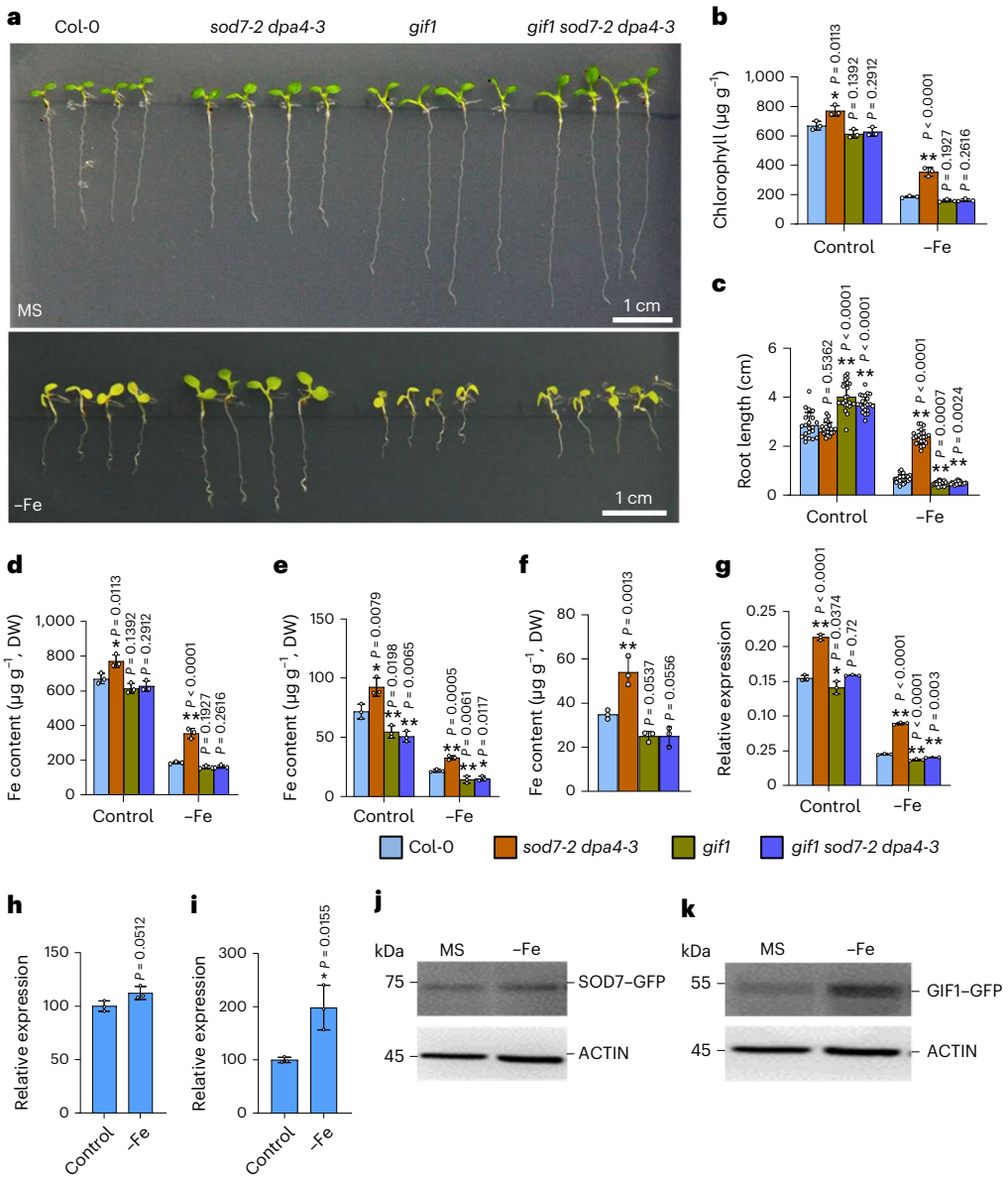

Fig. 4 | SOD7 and DPA4 negatively regulate Fe homeostasis. a, Seven-day seedlings of Col-0, *sod7-2 dpa4-3*, *gif1* and *gif1 sod7-2 dpa4-3* grown on MS or Fe-deficient (−Fe) medium. **b**, Chlorophyll content of 7 d seedlings grown on MS or −Fe medium ($n = 3$ biologically independent repeats). **c**, The relative root length of Col-0, *sod7-2 dpa4-3*, *gif1* and *gif1 sod7-2 dpa4-3* grown on MS or −Fe medium ($n = 22$ roots). **d**–**f**, The Fe content in roots (**d**), shoots (**e**) and seeds (**f**) of Col-0, *sod7-2 dpa4-3*, *gif1* and *gif1 sod7-2 dpa4-3* grown on MS or −Fe medium ($n = 3$ biologically independent repeats). **g**, The relative At*FER1* expression in roots of Col-0, *sod7-2 dpa4-3*, *gif1* and *gif1 sod7-2 dpa4-3* grown on MS or −Fe medium ($n = 3$ biologically independent repeats). **h**,**i**, The relative *SOD7* (**h**) and *GIF1* (**i**) expression in roots of Col-0 grown on MS and −Fe medium ($n = 3$ biologically independent repeats). **j**,**k**, The SOD7 (**j**) and GIF1 (**k**) protein level in roots of *SOD7–GFP* or *GIF1–GFP* transgenic plants grown on MS and −Fe medium. The experiments in **j** and **k** were repeated independently at least twice with similar results. Values represent mean ± s.d. Asterisks indicate significant differences, $^*P < 0.05$ and $^{**}P < 0.01$ compared with the wild type (one-way ANOVA with Dunnett's multiple comparisons test for **b**–**g**, and two-tailed unpaired *t*-test for **h** and **i**).

without Fe. Protein levels of SOD7–GFP and GIF1–GFP were detected using the GFP antibody. SOD7–GFP protein levels were similar when plants were grown on medium with or without Fe (Fig. 4j). By contrast, the GIF1–GFP protein level was obviously increased under Fe-deficient conditions, consistent with increased *GIF1* mRNA under the Fe-deficient conditions (Fig. 4i,k).

SOD7/DPA4–GIF1 regulates gene functions in Fe-deficiency pathway

The *sod7-2 dpa4-3* double mutant increased Fe accumulation and big organ formation, suggesting that Fe uptake in *sod7-2 dpa4-3* is enhanced. To test this, we examined the expression of Fe-uptake-related genes in Col-0, *sod7-2 dpa4-3*, *gif1* and *gif1 sod7-2 dpa4-3* plants grown on medium with or without Fe. The expression levels of *FRO2* and *IRT1*, two key Fe-uptake genes, and *FIT*, which is crucial in regulating the expression of Fe-uptake genes, were higher in *sod7-2 dpa4-3* than those in Col-0 under Fe-deficient conditions (Fig. 5a–c). By contrast, the expression levels of *FRO2*, *IRT1* and *FIT* in *gif1* and *gif1 sod7-2 dpa4-3* were dramatically decreased compared with those in Col-0 under Fe-deficient conditions (Fig. 5a–c). Expression levels of these three genes in *gif1 sod7-2 dpa4-3* were similar to those in *gif1* (Fig. 5a–c). In addition, six other Fe-responsive genes, including *bHLH100*, *NAS1*,

https://doi.org/10.1038/s41477-023-01475-0

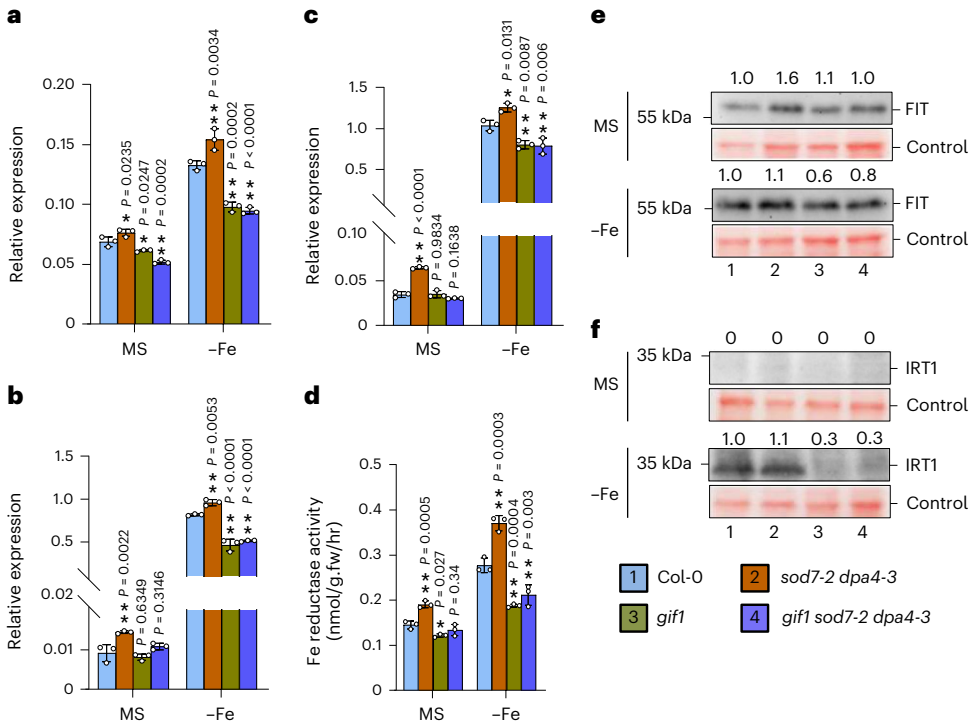

Fig. 5 | Characterization of Fe uptake activities in roots of wild-type and mutant plants. a–**c**, The relative expression levels of *FIT* (**a**), *FRO2* (**b**) and *IRT1* (**c**) in roots of wild-type and mutant plants grown on MS medium with or without 100 μM Fe. **d**, Quantification of ferric chelate reductase activity. **e**,**f**, Protein levels of FIT (**e**) and IRT1 (**f**) in roots of wild-type and mutant plants grown on MS medium with or without 100 μM Fe. After western blotting, the same membrane was stained with Ponceau S as a loading control. The numbers above the bands indicate the protein levels, with the respective Col-0 set as 1. The experiments in **e** and **f** were repeated independently at least twice with similar results. Data represent mean ± s.d., $n = 3$ for three biological replicates in **a**–**d**. Asterisks indicate significant differences, $^{*}P < 0.05$ and $^{**}P < 0.01$ compared with the wild type (one-way ANOVA with Dunnett's multiple comparisons test).

NAS2, *FRO3*, *MYB10* and *MYB72*, showed similar expression patterns to those of *FRO2*, *IRT1* and *FIT* in these mutants (Extended Data Fig. 8). These results supported that SOD7 and GIF1 act in a common pathway to participate in Fe uptake by influencing the expression of several Fe-uptake genes in *Arabidopsis*.

To verify the functions of *SOD7* and *GIF1* in regulating Fe uptake, we analysed ferric-chelate reductase (FCR) activity. When seedlings were grown on medium with Fe, the FCR activity in *sod7-2 dpa4-3* was higher than that in Col-0, consistent with high Fe accumulation in *sod7-2 dpa4-3* (Fig. 5d). Considering that FCR activity was induced in response to Fe deficiency, we compared the FCR activity in wild-type and mutant plants grown on medium without Fe. The FCR activity in *sod7-2 dpa4-3* was much higher than that in Col-0, which is consistent with high Fe accumulation in *sod7-2 dpa4-3* under Fe-deficient conditions (Fig. 5d). By contrast, *gif1* showed lower FCR activity than Col-0. The *gif1* mutation suppressed high FCR activity of *sod7-2 dpa4-3* under Fe-deficient conditions (Fig. 5d). These results further demonstrate that *SOD7* and *GIF1* function antagonistically in a common pathway to influence Fe uptake.

Considering that FIT and IRT1 accumulate under Fe-deficient conditions, we investigated levels of FIT and IRT1 in Col-0, *sod7-2 dpa4-3*, *gif1* and *gif1 sod7-2 dpa4-3* plants grown on MS medium with or without Fe supply. Importantly, the level of FIT in *sod7-2 dpa4-3* was higher than that in Col-0 when plants were grown on MS medium with Fe (Fig. 5e). The *gif1* mutation suppressed FIT accumulation in *sod7-2 dpa4-3* (Fig. 5e). When plants were grown on MS medium without Fe, *sod7-2 dpa4-3* kept the FIT level as high as Col-0, whereas the levels of FIT proteins were slightly lower in *gif1* and *gif1 sod7-2 dpa4-3* than that in Col-0 (Fig. 5e). Next, we analysed IRT1 levels. Consistent with a previous report[64], IRT1 was undetectable in plants grown on MS with Fe (Fig. 5f). Under Fe-deficient conditions, the level of IRT1 in *sod7-2 dpa4-3* was similar to that in Col-0, whereas levels of IRT1 in *gif1* and *gif1 sod7-2 dpa4-3* were much lower than that in Col-0 (Fig. 5f). Together, these results indicate that *sod7-2 dpa4-3* depends on functional GIF1 to retain high levels of FIT and IRT1. The levels of FIT and IRT1 proteins were associated with their mRNA expression levels (Fig. 5a,c).

GIF1 interacts with FIT to regulate Fe responses

Given that *SOD7* and *GIF1* regulate *FIT* transcription and protein levels, and FIT is a crucial regulator of Fe deficiency responses, we asked whether SOD7 and GIF1 could directly interact with FIT. To test this, we generated cYFP–SOD7, cYFP–GIF1 and nYFP–FIT and performed BiFC analysis. As shown in Extended Data Fig. 9, we did not observe any signal when cYFP–SOD7 and nYFP–FIT were coexpressed in *N. benthamiana* leaves. The Co-IP assay also confirmed that SOD7 did not interact with FIT (Fig. 6b). We then tested whether FIT could interact with the transcription coactivator GIF1 that usually interacts with the transcription factors to regulate gene expression. An in vitro pull-down assay was used to test their interaction. As shown in Fig. 6a, MBP–FIT was pulled down with GST–GIF1, but not with GST. We then conducted a Co-IP assay to verify the association of GIF1 with FIT in *Arabidopsis* plants. Total proteins were extracted from the roots of *35S:Myc–GIF1* and *35S:Myc–SOD7* transgenic plants and incubated with Myc beads. The immunoprecipitated proteins were detected by anti-Myc or anti-FIT antibodies. FIT was co-immunoprecipitated with Myc–GIF1, but not with Myc–SOD7, indicating that FIT interacts with GIF1 in *Arabidopsis* (Fig. 6b). We further generated cYFP–GIF1 and nYFP–FIT and conducted BiFC assays to confirm their interactions. Strong YFP fluorescence was detected in nuclei when cYFP–GIF1 and nYFP–FIT were coexpressed in *N. benthamiana* leaves, but not in the negative controls, indicating that

https://doi.org/10.1038/s41477-023-01475-0

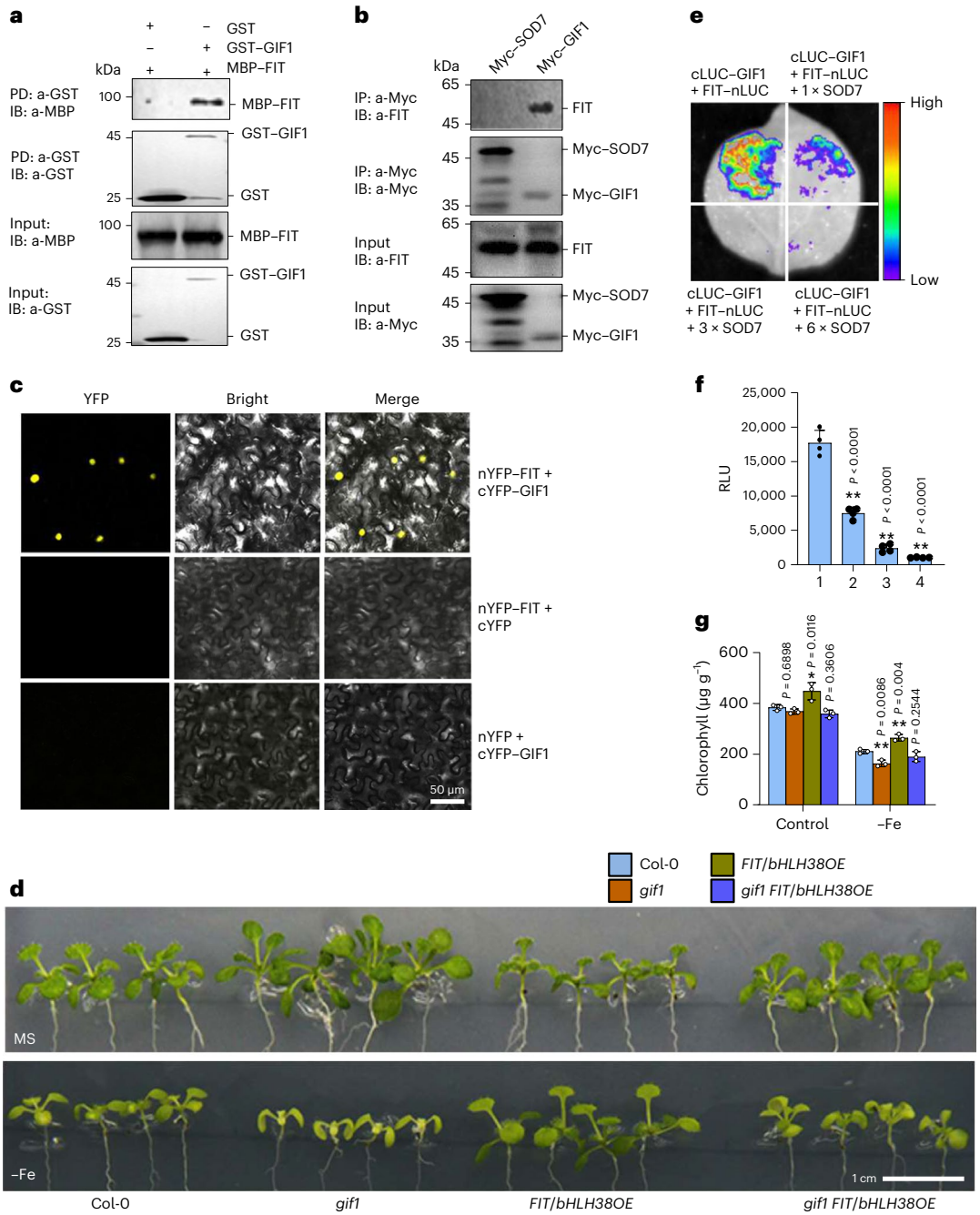

Fig. 6 | GIF1 interacts with FIT, and SOD7 competes that interaction. a, FIT interacts with GIF1 in pull-down assays. MBP–FIT was incubated with GST or GST–GIF1, as indicated. The interaction proteins were precipitated by GST beads and detected by anti-MBP or anti-GST antibodies. **b**, FIT interacts with GIF1 in a Co-IP analysis in *Arabidopsis*. Total protein extracted from roots of *35S:Myc–SOD7* and *35S:Myc–GIF1* transgenic plants grown under –Fe conditions was incubated with Myc agarose beads, and immunoblotting was used to detect the precipitates by anti-FIT or anti-Myc antibodies. The *35S:Myc–SOD7* plants were used as a negative control. **c**, FIT interacts with GIF1 in BiFC assays. Fluorescence indicates positive interactions. **d**, The 11 d seedlings of Col-0, *gif1*, *FIT/bHLH38OE* and *gif1 FIT/bHLH38OE* grown on MS or –Fe medium. The seeds were germinated and grown on MS medium for 7 d and then they were transferred to new MS or –Fe medium growing for another 4 d. **e**, SOD7 competes with the interaction between GIF1 and FIT detected by split luciferase complementation assays. *N. benthamiana* leaves were co-infiltrated with the *Agrobacterium* GV3101 containing combinations as indicated. The pseudocolour scale bar was used to indicate the range of luminescence intensity. **f**, Quantification of LUC signals from **e** ($n = 4$ biologically independent repeats); 1–4 represent samples with 0, 1, 3 and 6 × SOD7 added, respectively. **g**, Chlorophyll content of 11 d seedlings grown on MS or –Fe medium ($n = 3$ biologically independent repeats). Values represent mean ± s.d. Asterisks indicate significant difference, $^{*}P < 0.05$ and $^{**}P < 0.01$ compared with samples with no added *35S:SOD7* (**f**) or Col-0 (**g**) (one-way ANOVA with Dunnett's multiple comparisons test). The experiments in **a**–**c** were repeated at least three times with similar results.

GIF1 associates with FIT in nuclei (Fig. 6c). Thus, these results demonstrated that GIF1 interacts with FIT both in vitro and in vivo.

We then asked whether *GIF1* and *FIT* could function in a common pathway to influence Fe response. Considering that *35S:FIT* plants showed similar growth phenotypes to Col-0, while the double-overexpression plants (*FIT/bHLH38OE*) exhibited tolerance to Fe deficiency compared with Col-0 (refs. 45,47), we crossed the *gif1* mutant with *FIT/bHLH38OE* and generated *gif1 FIT/bHLH38OE*

plants. On MS medium with Fe, the colour of *gif1*, *FIT/bHLH38OE* and *gif1 FIT/bHLH38OE* leaves was similar to that of wild-type leaves (Fig. 6d). By contrast, *FIT/bHLH38OE* had more chlorophyll than Col-0 (Fig. 6g). Under Fe-deficient conditions, *gif1* showed pale green leaves and decreased chlorophyll compared with Col-0, whereas *FIT/bHLH38OE* plants had greener leaves and more chlorophyll than Col-0 (Fig. 6d,g), consistent with a previous report[47]. Importantly, the *gif1* mutation suppressed the phenotypes of *FIT/bHLH38OE* because *gif1 FIT/bHLH38OE* plants showed chlorosis in leaves and reduced chlorophyll compared with *FIT/bHLH38OE* plants, indicating that *FIT/bHLH38OE* plants need functional *GIF1* to promote chlorophyll accumulation in leaves (Fig. 6d,g).

SOD7 competitively represses the interaction of GIF1 and FIT

SOD7 physically interacts with GIF1 to regulate Fe uptake and responses, and FIT also interacts with GIF1. We, therefore, asked how these three proteins work together to influence Fe uptake and responses. It is possible that SOD7 could inhibit the interaction between GIF1 and FIT by competitively binding GIF1. To test this possibility, we coexpressed FIT–nLUC and cLUC–GIF1 with SOD7 in *N. benthamiana* leaves for 2 d. As we speculated, strong luciferase signals were detected when FIT–nLUC and cLUC–GIF1 were coexpressed (Fig. 6e,f). However, the luciferase signals decreased gradually with increasing SOD7 (Fig. 6e,f). We also coexpressed FIT–nLUC and cLUC–GIF1 with a negative control, GFP, and found that GFP did not influence the interaction between FIT and GIF1 (Extended Data Fig. 10). Thus, these results indicated that SOD7 competitively represses the interaction between GIF1 and FIT, thereby influencing Fe uptake and responses.

Discussion

Organ and seed size are important yield traits in plants. Understanding the genetic and molecular mechanisms underlying organ and seed size control will help to improve yield and biomass. Plant growth and development are strictly controlled by intrinsic genetic factors and external environmental signals, such as nutrient supply, light and temperature. It is fascinating to know how plants integrate organ growth with nutrient signalling. We have previously revealed that SOD7 regulates seed size by repressing expression of *KLU* in *Arabidopsis*[20]. In this study, we found that SOD7 interacts with the transcriptional coactivator GIF1 to coordinate organ and seed growth and Fe uptake by targeting several key regulators of growth and Fe uptake in *Arabidopsis*.

GIF1 has been reported to positively regulate leaf and seed size by influencing cell proliferation[25,31]. GIF1 normally forms complexes with GRF transcription factors to regulate plant growth and development. The combination of *gif* and *grf* mutations has a synergistic effect on the leaf size, and overexpression of both *GIF1* and *GRF3* synergistically increase leaf size, indicating that GIFs can boost GRFs' activity[25,27,65]. A recent study has revealed that the GIF–GRF chimeric protein can improve transgenic regeneration efficiency, further suggesting the importance of the GIF–GRF interation[66]. GIF1 has been reported to regulate seed size in *Arabidopsis* and rice[31,57,59]. Because functional redundancy exists among GRF family members, the role of loss of *GRF* function in seed size control has not been described in detail in *Arabidopsis*. In this study, we analysed the seed size of transgenic plants overexpressing *MIR396a* and *MIM396*. Our results reveal that transgenic plants overexpressing *MIR396a* produce small seeds, while plants overexpressing *MIM396* have large seeds (Fig. 3c,e). We also demonstrated that SOD7 competes with GRFs to interact with GIF1, resulting in the reduced levels of the GIF1–GRF complex (Fig. 3a,b and Extended Data Figs. 5 and 6). Our findings show a molecular mechanism in which SOD7 controls organ and seed size by competitively repressing the interaction between GIF1 and GRFs. GIF1 has been reported to associate with SWI–SNF chromatin remodeling complexes, such as SWP73A or SWP73B, SWI3C and/or SWI3D, and ARP4 and ARP7 around a central ATPase, BRM or SYD to regulate GRF3, 5, 6 and other gene transcriptions in leaf development[67]. It will be worth exploring whether SOD7 can influence the interaction between GIF1 and SWI–SNF complexes in regulation of organ growth in the future.

Plant growth is dependent on sufficient essential mineral nutrients and photosynthetic products. In the past, farmers pursued high yield by excessive use of synthetic chemical fertilizers, which caused severe environmental problems. Therefore, it is a big challenge for breeders to develop new cultivars with high yield at low nutrient supply. Plant organ and seed size correlate with crop yield. As the *sod7-2 dpa4-3* mutant produces bigger leaves and seeds than Col-0 (Fig. 2a,f), we proposed that the *sod7-2 dpa4-3* mutant may have better nutrient utilization. Consistent with this, *sod7-2 dpa4-3* contains more Fe, N, Ca and P than Col-0 in shoots, indicating that *sod7-2 dpa4-3* has better nutrient utilization (Supplementary Table 1). Considering that SOD7 and GIF1 act in a common pathway to regulate organ and seed size, we simultaneously analysed the elemental composition of *gif1* and *gif1 sod7-2 dpa4-3*. Consistent with the relationship between SOD7 and GIF1 in organ and seed size control, SOD7 functions antagonistically with GIF1 in a common pathway to regulate the Fe accumulation. Supporting this notion, the *sod7-2 dpa4-3* mutant displayed tolerance to Fe deficiency, while *gif1* and *gif1 sod7-2 dpa4-3* were sensitive to Fe deficiency (Fig. 4a–c). Expressions of *FIT*, *IRT1* and *FRO2*, which are key genes involved in the Fe-deficiency-response pathway, were highly upregulated in *sod7-2 dpa4-3*, whereas *gif1* suppressed the expression of these genes in *sod7-2 dpa4-3* mutants (Fig. 5a–c). We further revealed that SOD7 regulates Fe uptake by competitively repressing the interaction between GIF1 and FIT (Fig. 6e,f). FIT has been reported to form heterodimers with members of subgroup Ib bHLH transcription factor in the regulation of Fe deficiency responses[47]. It will be interesting to investigate whether GIF1 could interact with the subgroup Ib bHLH family members or other key transcription factors involved in the Fe-deficiency-response pathway in the future. We also found that there is more N, Ca and P in *sod7-2 dpa4-3* mutant than those in the wild type, but the changes of these elemental concentrations in *sod7-2 dpa4-3* did not depend on the *GIF1* function (Supplementary Table 1). It will be a worthwhile challenge to understand how SOD7 and DPA4 regulate the homeostasis of these elements in the future because they are essential nutrients for plant growth and development.

Based on our genetic and biochemical data, we proposed a working model for SOD7/DPA4–GIF1-mediated control of organ growth and Fe utilization. In the wild type, SOD7 limits organ growth by competitively repressing the interaction between GIF1 and GRFs. SOD7 can also regulate Fe uptake by competitively repressing the interaction between GIF1 and FIT. In the *sod7-2 dpa4-3* double mutant, which loses the function of SOD7 and DPA4, the interactions of GIF1 with GRFs or FIT were enhanced, thereby promoting organ growth and Fe uptake (Fig. 7). Thus, our findings reveal a coordinated mechanism for plant organ growth and Fe uptake. Considering that SOD7 protein level was not influenced when plants are grown on medium with or without Fe (Fig. 4k), it raised a question how SOD7 coordinates plant growth and Fe uptake. We speculated that the interaction between SOD7 and GIF1 might be changed under Fe-deficient conditions. Supporting this, the interaction between SOD7 and GIF1 was decreased under Fe-deficient condition (Supplementary Fig. 1), indicating that SOD7 possibly coordinates plant growth and Fe uptake by influencing its interaction with GIF1 in response to Fe deficiency. Considering that FIT was induced under Fe-deficient conditions, it is possible that the Fe deficiency may promote the interaction between GIF1 and FIT to fit the stress condition. It will be a difficult but worthwhile challenge to investigate how GIF1 interacts with GRFs and FIT to fine tune organ growth and Fe uptake in the future.

With the rapid development of molecular design breeding, researchers can accelerate the breeding processes to cultivate desired varieties. Our work revealed that the SOD7/DPA4–GIF1 module simultaneously regulates organ and seed growth and Fe uptake by recruiting

https://doi.org/10.1038/s41477-023-01475-0

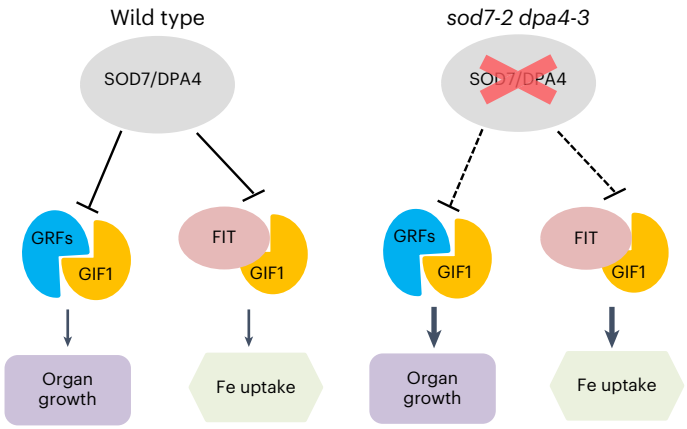

Fig. 7 | A proposed model for the SOD7/DPA4–GIF1 module coordinating organ growth and Fe uptake in *Arabidopsis*. In this model, SOD7 interacts with GIF1 to regulate organ growth and Fe responses through recruiting different members. In the wild type, SOD7 limits the organ growth through competitively repressing the interaction between GIF1 and GRFs. SOD7 can simultaneously regulate Fe uptake through competitively repressing the interaction between GIF1 and FIT. However, in *sod7-2 dpa4-3*, because the lost function of SOD7 and DPA4, the interaction between GIF1 and GRFs or GIF1 and FIT was enhanced, thereby promoting organ growth and Fe uptake.

GRF organ growth regulators and the Fe-uptake regulator FIT, suggesting that this module is a promising target for improving both yield and nutrient utilization efficiency. OsGIF1, the homologue of GIF1 in rice, has been reported to promote grain growth[57,59]. Homologues of GIF1 and SOD7 also exist in crops. It will be interesting to investigate whether homologues of SOD7 and GIF1 in key crops could coordinate organ growth and Fe uptake and be used to improve both yield and nutrient utilization efficiency in the future.

Methods

Plant materials and growth conditions

All plant materials were in Col-0 background. The *sod7-2* (SM_3.34191) *dpa4-3* (SM_3.36641), *gif1* (SALK_150407), *proSOD7:SOD7:GFP* and *proGIF1:GIF1:GFP* plants[20,31]; the transgenic lines of *35S:miR396a* and *35S:MIM396*[61]; and the *FIT/bHLH38OE* transgenic line have all been reported previously[47]. The *gif1 sod7-2 dpa4-3* triple mutant was obtained by crossing *sod7-2 dpa4-3* with *gif1* and isolated by polymerase chain reaction (PCR) using T-DNA specific and flanking primers as listed in Supplementary Table 2.

Seeds were put on filter paper and surface sterilized with hydrogen peroxide and 85% (v/v) ethanol (1:4) in a sterile hood. The dried seeds were plated on solid MS medium with 1% sucrose. After stratification at 4 °C in the dark for 3 d, the seeds were germinated at 22 °C with 16 h light followed by 8 h dark. The 7 d seedlings were then transferred to soil in the greenhouse under long-day conditions (22 °C; 16 h light, 8 h dark).

Constructs for transgenic plants

The GBclonart Seamless Clone Kit (GB2001-48, Genebank Biosciences) was used to generate all constructs. Primers for cloning are listed in Supplementary Table 2. We amplified whole coding sequences (CDS) of *SOD7* and *GIF1* and inserted into the pCambia1300-221-Myc vector (double digested by restriction enzymes BamHI and PacI) to generate *35S:Myc–SOD7* and *35S:Myc–GIF1*, respectively. For *35S:GFP–GIF1* recombinant construct, the CDS of *GIF1* was cloned and fused into pMDC43 vector (double digested by restriction enzymes AscI and PacI).

Yeast two-hybrid assay

To validate the interaction between SOD7 and GIF1, the Invitrogen Yeast Two-Hybrid System was used to perform a yeast two-hybrid assay. Full-length CDS or fragments of *SOD7* were fused into bait vector pDBleu (double digested by restriction enzymes NotI and SalI) and *GIF1* CDS was cloned to prey vector pEXP-AD502 (double digested by restriction enzymes NotI and SalI). The plasmids were co-transformed into yeast strain AH109 and grown on yeast SD-2 selective medium at 30 °C for approximately 3 d. The largest colonies were selected and spotted on fresh SD-2 and SD-4 plates with dilutions for selecting true interactions. The plates were incubated for 3 or more days at 30 °C before the photos of positive clones were taken using a camera. Primers used for constructing vectors are listed in Supplementary Table 2.

Pull-down assays

To confirm the interaction between SOD7 and GIF1–3; DPA4 and GIF1–3; and GIF1 and FIT, the CDSs of *GIF1–3* were inserted into *pGEX-4T-1* vector (double digested by restriction enzymes EcoRI and SalI) to construct GST–GIF1–3 plasmids, while the CDSs of *SOD7*, *DPA4* and *FIT* were inserted into *pMAL-c2* vector (double digested by restriction enzymes SalI and HindIII) to construct MBP–SOD7, MBP–DPA4 and MBP–FIT plasmids by GBclonart Seamless Clone Kit. Plasmids were introduced into *Escherichia coli* BL21 (DE3) cells. The expression of corresponding proteins was induced with 0.5 mM isopropyl β-D-1-thiogalactopyranoside at 28 °C for 3 h. Appropriate bacterial lysate combinations in TGH buffer (50 mM HEPES pH 7.5, 1% Triton X-100, 5 mM $MgCl_2$, 1 mM EGTA, 150 mM NaCl, and 10% glycerol) were incubated and pulled down by 20 µl MBP beads (amylase resin, New England Biolabs) or GST beads (Glutathione Sepharose 4B, GE Healthcare) with gentle shaking at 4 °C for 1 h. The TGH buffer was used to wash beads five times. The beads were then added to 50 µl 1X SDS-loading buffer and boiled for 5 min at 98 °C. The eluted proteins were separated by 10% SDS–PAGE gel and then transferred to membrane and detected with anti-GST (1:5,000, Abmart, M20007) or anti-MBP antibodies (1:10,000, NEB, #E8032).

Co-immunoprecipitation

To test protein interactions in vivo, a Co-IP assay was performed as described previously[68]. *N. benthamiana* leaves were co-transformed with *Agrobacterium* GV3101 cells harbouring different combinations of *35 S:GFP*, *35 S:GFP–GIF1* and *35 S:Myc–SOD7* plasmids and grown in the greenhouse for 3d. For SOD7 competitively repressing the interaction between GIF1 and GRFs in vivo, different combinations of *35 S: GFP-rGRF2*, *35 S: Myc-GIF1*, *35 S: Myc–SOD7* and *35 S: Myc-TCP15* were transiently overexpressed in *N. benthamiana* leaves. Total proteins were extracted with the buffer (50 mM Tris-HCl pH 7.4, 10% glycerol, 1 mM EDTA, 2%Triton X-100, 150 mM NaCl, 1X Complete protease inhibitor cocktail) and incubated with GFP–Trap-A agarose (Chromotek gta-20) on the rotator in cold room for 0.5 h. Beads were washed three times with the buffer containing 50 mM Tris-HCl (pH 7.4), 10% (v/v) glycerol, 1 mM EDTA, 150 mM NaCl, 0.5% (v/v) Triton X-100 and 1X protease inhibitor cocktail. The beads were then boiled for 5 min after adding 40 µl 1X SDS-loading buffer. The immunoprecipitates were separated by 10% SDS–PAGE gel and detected by anti-GFP (Abmart M20004, 1:5,000) and anti-Myc (Abmart M20002, 1:5,000) antibodies. For detection the interaction between GIF1 and FIT, the transgenic *Arabidopsis* plants expressing *35S:Myc*-GIF1 or *35S:Myc–SOD7* (negative control) were used to extract the total proteins. The proteins were mixed with 20 µl Myc beads and incubated for 1 h at 4 °C with agitation. After three washes, the samples were detected by western blot with anti-Myc (Abmart, M20002, 1:5,000) or anti-FIT antibody[69].

Morphological and cellular analysis

Cotyledons were detached from 7–8 d seedlings, the sixth mature leaves were harvested and photographed as digital images for measuring the surface area, length and width using ImageJ software. For leaf cell size and number, the sixth mature leaves were cleared in clearing solution (30 ml water, 10 ml glycerol, 80 g chloral hydrate). From the

cleared materials were taken micrographs by a microscope (Leica DM2500) with a digital image system. Leaf palisade cell numbers and size in the maximum-width region were determined by ImageJ.

For seed size analysis, the mature seeds of wild-type and mutant plants were harvested from the fourth to twelfth silique on the main stem of plants. The seed area was then obtained by ImageJ after being photographed using a microscope (Leica S8APO) with CCD imaging apparatus. The observation of seed integument was described previously with slight modifications[31]. In brief, we artificially pollinated the fourth flower on the main stem of plants and harvested the seeds at 0 and 6 DAP. Next, the seeds were fixed with FAA solution (70% ethanol, 37% formaldehyde, 5 ml acetic acid; 18:1:1), and then cleared with clearing solution (30 ml water, 10 ml glycerol, 80 g chloral hydrate) before they were observed under the differential interference contrast microscope (DM2500, Leica).

For root length measurements, we grew seedlings vertically on MS medium with 1% sucrose, supplied with or without 100 μM Fe-EDTA for 7 d. Digital photos of the roots were taken and root lengths were obtained by ImageJ software.

Split luciferase complementation assays

The assay was performed as reported previously[70], we generated cLUC–SOD7, cLUC–DPA4, cLUC–GRF2/GRF3, FIT–nLUC, GIF2–nLUC, GIF3–nLUC, cLUC–GIF1 and GIF1–nLUC by fusing the respective CDS into *pCAMBIA-split_cLUC* and *pCAMBIA-split_nLUC* vectors. All the primers used for cloning are listed in Supplementary Table 2. Sequencing corrected plasmids were transformed into *Agrobacterium tumefaciens* strain GV3101. Different overnight cultured GV3101 cells were mixed as indicated combinations to a final OD_{600} = 0.5. The mixtures were immediately centrifuged at 5,000*g* for 15 min at room temperature and resuspended in activation buffer (10 mM MES, pH 5.7, 150 μM acetosyringone and 10 mM $MgCl_2$). After incubation for at least 2 h at room temperature with gentle agitation, the activated GV3101 cells were transformed into *N. benthamiana* leaves and expressed for another 2–3 d before the LUC activity measurement. To treat plants with or without Fe, the roots of plants after transformation were grown in liquid MS supplied with or without Fe for another 3 d before the LUC activity measurement. For observing the LUC signals, 1 mM D-luciferin solution (E1602, Promega) was sprayed onto the leaves of *N. benthamiana* and they were kept in the dark for 5 min. The images were captured by a NightOWL II LB 983 imaging apparatus with CCD.

To quantify the LUC signals, same size leaf discs were made to incubate with 1 mM D-luciferin in a Microplate (Corning) for 5–10 min. We measured the luminescence activity using a microplate luminometer (Promega, GLOMAX 96). Each sample was measured with at least four independent repeats.

Fe content measurement

The roots and shoots of 10-day-old seedlings grown on medium as indicated were harvested separately to measure Fe content. We also harvested the mature seeds for the same purpose. The samples were first immersed in $CaSO_4$·EDTA solution (5 mM $CaSO_4$, 10 mM EDTA·$2H_2O$) for 5 min to remove surface-attached ions, and then washed 3 times with sterile water. Next, the samples were incubated at 120 °C for 30 min, then 65 °C for 3 days for completely dehydration. Subsequently, dried samples were weighed and digested in a nitric acid and hydrogen peroxide solution (mixed at a 10:2 ratio) at 140 °C for 1 h in an ETHOS1 Microwave Digestion System (Milestone). The content of Fe in solutions was determined by inductively coupled plasma-optic emission spectroscopy (model 5300DV, Perkin Elmer).

Assay of root FCR activity

The assay of FCR activity was performed from whole intact roots as described previously[71]. Roots of seedlings grown on MS medium with or without 100 μM Fe-EDTA supply for 10 d were harvested and rinsed with distilled pure water. The roots were then put on assay plates (1/2 MS Macroelement, 100 μM Fe(III)NaEDTA, 200 μM BPDS (bathophenanthrolinedisulfonate), 0.6% phytogel, pH 5.5) or submerged in assay solution (200 μM $CaSO_4$, 100 μM Fe(III)NaEDTA, 200 μM BPDS, 5 mM MES, pH 5.5). After 1 h, an aliquot of the assay solution was removed and its absorbance was determined with a spectrometer at 535 nm wavelength. The Fe(II)-BPDS concentration was calculated by using the extinction coefficient of 22.14 mM^{-1} cm^{-1}. The experiment was independently repeated three times.

Bimolecular fluorescence complementation assay

The coding sequence of *FIT* was amplified and fused with the N-terminal fragment of YFP (nYFP) to generate FIT–nYFP. The CDS of *GIF1* and *SOD7* were amplified and ligated to the C-terminal fragment of YFP (cYFP) to generate GIF1–cYFP and SOD7–cYFP, respectively. All the plasmids were subsequently transferred into *Agrobacterium* strain GV3101. The various combinations of *Agrobacterium* cells were infiltrated into leaves of 4-week-old *N. benthamiana* plants. The YFP fluorescence was detected after 2 d infiltration using a Leica SP8 confocal microscope system. All the primers used for cloning are listed in Supplementary Table 2.

RNA isolation, reverse transcription and quantitative real-time PCR assays

Total RNA was isolated using RNAprep pure kit (TIANGEN, DP432) and cDNA synthesis was performed with HiScript II Q RT SuperMix for qPCR (+gDNA wiper; Vazyme). The qRT-PCR was then analysed using RealStar Green Fast Mixture (GenStar) on Realplex2 machine (Eppendorf). The data were calculated by the cycle threshold method and averaged by three biological replicates. The internal control was *ACTIN2*. The primers used for qRT-PCR reactions are listed in Supplementary Table 2.

Chlorophyll measurement

The 7 d old shoots of Col-0, *sod7-2 dpa4-3*, *gif1* and *gif1 sod7-2 dpa4-3* grown on MS supplied with or without Fe were collected for chlorophyll measurement. For chlorophyll measurement of Col-0, *gif1*, *FIT/bHLH38OE* and *gif1 FIT/bHLH38OE*, the plants were first grown on MS for 7 d and then transferred to new MS with or without Fe for another 4 d. The fresh weights of all samples were determined before we extracted the chlorophyll in 10 ml of 90% acetone in the dark at room temperature for 24 h. The supernatant was then used to measure the chlorophyll content at 647 and 664 nm by spectrophotometry[72].

Protoplast preparation

The rosette leaves of *sod7-2 dpa4-3* harvested before bolting were used to isolate protoplast. The leaves were fragmented and incubated in enzyme solution (0.3% Macerozyme R-10, 20 mM MES at pH 5.7, 1.25% Cellulose RS, 10 mM $CaCl_2$, 0.4 M mannitol, 0.1% BSA and 5 mM β-mercaptoethanol) with gentle shaking for 4 h in the dark. The digestion solution was then mixed with the same volume of W5 solution (154 mM NaCl, 125 mM $CaCl_2$, 5 mM KCl and 2 mM MES at pH 5.7) and rotated vigorously for 10–30 s. Protoplasts were isolated through 40 μm nylon mesh filter with three washes of W5 solution. After centrifugation at 100*g* for 3 min and repeat twice washing with W5 solution, the pellets were collected and suspended in MMG solution (4 mM MES at pH 5.7, 0.4 M mannitol, and 15 mM $MgCl_2$) to 2×10^6 protoplasts ml^{-1}.

The CDS of *GIF1* was cloned to *PE3308* vector for GIF1–nVenus. The CDS of rGRF2/3 was fused to *PE3449* vector for rGRF2/3–cCFP (refs. 73,74). The plasmids were extracted with Plasmid Maxprep Kit (Vigorous). The combinations of plasmids as indicated were mixed with 400 μl protoplasts and 480 μl freshly prepared polyethylene glycol solution (40% w/v PEG4000, 0.4 M mannitol, 0.1 M $CaCl_2$). The protoplasts were then incubated at room temperature for 20 min. After serial dilutions with W5 solution, the transfected protoplasts were centrifuged and resuspended in W5 solution and cultured for 16 h at 23 °C in the dark.

Reporting summary

Further information on research design is available in the Nature Portfolio Reporting Summary linked to this article.

Data availability

All materials in this study are available from the corresponding authors upon request. The authors declare that all data supporting the findings of this study are available within the article and its supplementary information files. *Arabidopsis* reference genome (TAIR10) was used in this study. The primers used in this study are provided as Supplementary Table 2. Source data are provided with this paper.

References

1. Czesnick, H. & Lenhard, M. Size control in plants–lessons from leaves and flowers. *Cold Spring Harb. Perspect. Biol.* **7**, a019190 (2015).
2. Bogre, L., Magyar, Z. & Lopez-Juez, E. New clues to organ size control in plants. *Genome Biol.* **9**, 226 (2008).
3. Li, N., Xu, R. & Li, Y. Molecular networks of seed size control in plants. *Annu Rev. Plant Biol.* **70**, 435–463 (2019).
4. Ingram, G. C. & Waites, R. Keeping it together: co-ordinating plant growth. *Curr. Opin. Plant Biol.* **9**, 12–20 (2006).
5. Mizukami, Y. A matter of size: developmental control of organ size in plants. *Curr. Opin. Plant Biol.* **4**, 533–539 (2001).
6. Horiguchi, G., Ferjani, A., Fujikura, U. & Tsukaya, H. Coordination of cell proliferation and cell expansion in the control of leaf size in *Arabidopsis thaliana*. *J. Plant Res.* **119**, 37–42 (2006).
7. Li, S. et al. The plant-specific G protein γ subunit AGG3 influences organ size and shape in *Arabidopsis thaliana*. *N. Phytol.* **194**, 690–703 (2012).
8. Li, N. & Li, Y. Signaling pathways of seed size control in plants. *Curr. Opin. Plant Biol.* **33**, 23–32 (2016).
9. Li, N. & Li, Y. Maternal control of seed size in plants. *J. Exp. Bot.* **66**, 1087–1097 (2015).
10. Huang, L. et al. The LARGE2-APO1/APO2 regulatory module controls panicle size and grain number in rice. *Plant Cell* **33**, 1212–1228 (2021).
11. Lyu, J. et al. Control of grain size and weight by the GSK2-LARGE1/OML4 pathway in rice. *Plant Cell* **32**, 1905–1918 (2020).
12. Swaminathan, K., Peterson, K. & Jack, T. The plant B3 superfamily. *Trends Plant Sci.* **13**, 647–655 (2008).
13. Kim, S., Soltis, P. S., Wall, K. & Soltis, D. E. Phylogeny and domain evolution in the *APETALA2*-like gene family. *Mol. Biol. Evol.* **23**, 107–120 (2006).
14. Xia, F. et al. Insight into the B3 transcription factor superfamily and expression profiling of *B3* genes in axillary buds after topping in tobacco (*Nicotiana tabacum* L.). *Genes* **10**, 164 (2019).
15. Alvarez, J. P. et al. Endogenous and synthetic microRNAs stimulate simultaneous, efficient, and localized regulation of multiple targets in diverse species. *Plant Cell* **18**, 1134–1151 (2006).
16. Alvarez, J. P., Goldshmidt, A., Efroni, I., Bowman, J. L. & Eshed, Y. The *NGATHA* distal organ development genes are essential for style specification in *Arabidopsis*. *Plant Cell* **21**, 1373–1393 (2009).
17. Fourquin, C. & Ferrandiz, C. The essential role of NGATHA genes in style and stigma specification is widely conserved across eudicots. *N. Phytol.* **202**, 1001–1013 (2014).
18. Lee, B. H. et al. The *Arabidopsis thaliana* NGATHA transcription factors negatively regulate cell proliferation of lateral organs. *Plant Mol. Biol.* **89**, 529–538 (2015).
19. Shao, J., Liu, X., Wang, R., Zhang, G. & Yu, F. The over-expression of an Arabidopsis B3 transcription factor, ABS2/NGAL1, leads to the loss of flower petals. *PLoS ONE* **7**, e49861 (2012).
20. Zhang, Y. et al. Transcription factors SOD7/NGAL2 and DPA4/NGAL3 act redundantly to regulate seed size by directly repressing *KLU* expression in *Arabidopsis thaliana*. *Plant Cell* **27**, 620–632 (2015).
21. Shao, J. et al. NGATHA-LIKEs control leaf margin development by repressing *CUP-SHAPED COTYLEDON2* transcription. *Plant Physiol.* **184**, 345–358 (2020).
22. Liebsch, D. & Palatnik, J. F. MicroRNA miR396, GRF transcription factors and GIF co-regulators: a conserved plant growth regulatory module with potential for breeding and biotechnology. *Curr. Opin. Plant Biol.* **53**, 31–42 (2020).
23. Kim, J. H. Biological roles and an evolutionary sketch of the GRF-GIF transcriptional complex in plants. *BMB Rep.* **52**, 227–238 (2019).
24. Lee, G.-H. et al. Systematic assessment of the positive role of *Arabidopsis thaliana* GROWTH-REGULATING FACTORs in regulation of cell proliferation during leaf growth. *J. Plant Biol.* **65**, 413–422 (2022).
25. Horiguchi, G., Kim, G. T. & Tsukaya, H. The transcription factor AtGRF5 and the transcription coactivator AN3 regulate cell proliferation in leaf primordia of *Arabidopsis thaliana*. *Plant J.* **43**, 68–78 (2005).
26. Kim, J. H., Choi, D. & Kende, H. The AtGRF family of putative transcription factors is involved in leaf and cotyledon growth in *Arabidopsis*. *Plant J.* **36**, 94–104 (2003).
27. Kim, J. H. & Kende, H. A transcriptional coactivator, AtGIF1, is involved in regulating leaf growth and morphology in *Arabidopsis*. *Proc. Natl Acad. Sci. USA* **101**, 13374–13379 (2004).
28. Lee, B. H. et al. The Arabidopsis *GRF-INTERACTING FACTOR* gene family performs an overlapping function in determining organ size as well as multiple developmental properties. *Plant Physiol.* **151**, 655–668 (2009).
29. Ercoli, M. F. et al. GIF transcriptional coregulators control root meristem homeostasis. *Plant Cell* **30**, 347–359 (2018).
30. Kim, J. H. & Tsukaya, H. Regulation of plant growth and development by the GROWTH-REGULATING FACTOR and GRF-INTERACTING FACTOR duo. *J. Exp. Bot.* **66**, 6093–6107 (2015).
31. Liu, Z., Li, N., Zhang, Y. & Li, Y. Transcriptional repression of *GIF1* by the KIX-PPD-MYC repressor complex controls seed size in Arabidopsis. *Nat. Commun.* **11**, 1846 (2020).
32. Lee, B. H. et al. The *Arabidopsis thaliana GRF-INTERACTING FACTOR* gene family plays an essential role in control of male and female reproductive development. *Dev. Biol.* **386**, 12–24 (2014).
33. Liang, G., He, H., Li, Y., Wang, F. & Yu, D. Molecular mechanism of microRNA396 mediating pistil development in Arabidopsis. *Plant Physiol.* **164**, 249–258 (2014).
34. Jones-Rhoades, M. W. & Bartel, D. P. Computational identification of plant microRNAs and their targets, including a stress-induced miRNA. *Mol. Cell* **14**, 787–799 (2004).
35. Rodriguez, R. E. et al. Control of cell proliferation in *Arabidopsis thaliana* by microRNA miR396. *Development* **137**, 103–112 (2010).
36. Liu, D., Song, Y., Chen, Z. & Yu, D. Ectopic expression of miR396 suppresses GRF target gene expression and alters leaf growth in *Arabidopsis*. *Physiol. Plant.* **136**, 223–236 (2009).
37. Beltramino, M. et al. Robust increase of leaf size by *Arabidopsis thaliana GRF3*-like transcription factors under different growth conditions. *Sci. Rep.* **8**, 13447 (2018).
38. Briat, J. F., Dubos, C. & Gaymard, F. Iron nutrition, biomass production, and plant product quality. *Trends Plant Sci.* **20**, 33–40 (2015).
39. Jeong, J. & Guerinot, M. L. Homing in on iron homeostasis in plants. *Trends Plant Sci.* **14**, 280–285 (2009).
40. Balk, J. & Schaedler, T. A. Iron cofactor assembly in plants. *Annu Rev. Plant Biol.* **65**, 125–153 (2014).
41. Connorton, J. M., Balk, J. & Rodriguez-Celma, J. Iron homeostasis in plants—a brief overview. *Metallomics* **9**, 813–823 (2017).
42. Santi, S. & Schmidt, W. Dissecting iron deficiency-induced proton extrusion in Arabidopsis roots. *N. Phytol.* **183**, 1072–1084 (2009).

43. Robinson, N. J., Procter, C. M., Connolly, E. L. & Guerinot, M. L. A ferric-chelate reductase for iron uptake from soils. *Nature* **397**, 694–697 (1999).
44. Eide, D., Broderius, M., Fett, J. & Guerinot, M. L. A novel iron-regulated metal transporter from plants identified by functional expression in yeast. *Proc. Natl Acad. Sci. USA* **93**, 5624–5628 (1996).
45. Colangelo, E. P. & Guerinot, M. L. The essential basic helix-loop-helix protein FIT1 is required for the iron deficiency response. *Plant Cell* **16**, 3400–3412 (2004).
46. Ling, H. Q., Bauer, P., Bereczky, Z., Keller, B. & Ganal, M. The tomato *fer* gene encoding a bHLH protein controls iron-uptake responses in roots. *Proc. Natl Acad. Sci. USA* **99**, 13938–13943 (2002).
47. Yuan, Y. et al. FIT interacts with AtbHLH38 and AtbHLH39 in regulating iron uptake gene expression for iron homeostasis in *Arabidopsis*. *Cell Res* **18**, 385–397 (2008).
48. Wang, N. et al. Requirement and functional redundancy of Ib subgroup bHLH proteins for iron deficiency responses and uptake in *Arabidopsis thaliana*. *Mol. Plant* **6**, 503–513 (2013).
49. Yu, F. et al. FERONIA receptor kinase controls seed size in *Arabidopsis thaliana*. *Mol. Plant* **7**, 920–922 (2014).
50. Li, Y., Zheng, L., Corke, F., Smith, C. & Bevan, M. W. Control of final seed and organ size by the *DA1* gene family in *Arabidopsis thaliana*. *Genes Dev.* **22**, 1331–1336 (2008).
51. Baloban, M. et al. Complementary and dose-dependent action of AtCCS52A isoforms in endoreduplication and plant size control. *N. Phytol.* **198**, 1049–1059 (2013).
52. Tsukaya, H. Interpretation of mutants in leaf morphology: genetic evidence for a compensatory system in leaf morphogenesis that provides a new link between cell and organismal theories. *Int Rev. Cytol.* **217**, 1–39 (2002).
53. Van Daele, I. et al. A comparative study of seed yield parameters in *Arabidopsis thaliana* mutants and transgenics. *Plant Biotechnol. J.* **10**, 488–500 (2012).
54. Hong, J. K. et al. Overexpression of *Brassica rapa GROWTH-REGULATING FACTOR* genes in *Arabidopsis thaliana* increases organ growth by enhancing cell proliferation. *J. Plant Biotechnol.* **44**, 271–286 (2017).
55. Liu, J. et al. The *BnGRF2* gene (*GRF2-like* gene from *Brassica napus*) enhances seed oil production through regulating cell number and plant photosynthesis. *J. Exp. Bot.* **63**, 3727–3740 (2012).
56. Chen, X. et al. A missense mutation in *Large Grain Size 1* increases grain size and enhances cold tolerance in rice. *J. Exp. Bot.* **70**, 3851–3866 (2019).
57. Duan, P. et al. Regulation of *OsGRF4* by OsmiR396 controls grain size and yield in rice. *Nat. Plants* **2**, 15203 (2015).
58. Hu, J. et al. A rare allele of *GS2* enhances grain size and grain yield in rice. *Mol. Plant* **8**, 1455–1465 (2015).
59. Li, S. et al. The OsmiR396c-OsGRF4-OsGIF1 regulatory module determines grain size and yield in rice. *Plant Biotechnol. J.* **14**, 2134–2146 (2016).
60. Sun, P. et al. *OsGRF4* controls grain shape, panicle length and seed shattering in rice. *J. Integr. Plant Biol.* **58**, 836–847 (2016).
61. Wang, L. et al. The miR396-GRFs module mediates the prevention of photo-oxidative damage by brassinosteroids during seedling de-etiolation in Arabidopsis. *Plant Cell* **32**, 2525–2542 (2020).
62. Petit, J. M., Briat, J. F. & Lobreaux, S. Structure and differential expression of the four members of the Arabidopsis thaliana ferritin gene family. *Biochem. J.* **359**, 575–582 (2001).
63. Murgia, I. et al. Knock-out of ferritin *AtFer1* causes earlier onset of age-dependent leaf senescence in *Arabidopsis*. *Plant Physiol. Biochem.* **45**, 898–907 (2007).
64. Connolly, E. L., Fett, J. P. & Guerinot, M. L. Expression of the IRT1 metal transporter is controlled by metals at the levels of transcript and protein accumulation. *Plant Cell* **14**, 1347–1357 (2002).
65. Debernardi, J. M. et al. Post-transcriptional control of *GRF* transcription factors by microRNA miR396 and GIF co-activator affects leaf size and longevity. *Plant J.* **79**, 413–426 (2014).
66. Debernardi, J. M. et al. A GRF–GIF chimeric protein improves the regeneration efficiency of transgenic plants. *Nat. Biotechnol.* **38**, 1274–1279 (2020).
67. Vercruyssen, L. et al. ANGUSTIFOLIA3 binds to SWI/SNF chromatin remodeling complexes to regulate transcription during *Arabidopsis* leaf development. *Plant Cell* **26**, 210–229 (2014).
68. Hao, J. et al. The GW2-WG1-OsbZIP47 pathway controls grain size and weight in rice. *Mol. Plant* **14**, 1266–1280 (2021).
69. Cui, Y. et al. Four IVa bHLH transcription factors are novel interactors of FIT and mediate JA inhibition of iron uptake in *Arabidopsis*. *Mol. Plant* **11**, 1166–1183 (2018).
70. Wu, L. et al. A natural allele of *OsMS1* responds to temperature changes and confers thermosensitive genic male sterility. *Nat. Commun.* **13**, 2055 (2022).
71. Zhang, Y. et al. Mediator subunit 16 functions in the regulation of iron uptake gene expression in Arabidopsis. *N. Phytol.* **203**, 770–783 (2014).
72. Khan, M. S. et al. Crosstalk between iron and sulfur homeostasis networks in *Arabidopsis*. *Front. Plant Sci.* **13**, 878418 (2022).
73. Li, C. et al. *FERONIA* is involved in *phototropin 1*-mediated blue light phototropic growth in *Arabidopsis*. *J. Integr. Plant Biol.* **64**, 1901–1915 (2022).
74. Yu, F. et al. FERONIA receptor kinase pathway suppresses abscisic acid signaling in *Arabidopsis* by activating ABI2 phosphatase. *Proc. Natl Acad. Sci. USA* **109**, 14693–14698 (2012).

Acknowledgements

We thank Jianmin Zhou (Institute of Genetics and Developmental Biology, CAS) for kindly providing the split luciferase complementation vectors, Mingyi Bai (School of Life Science, Shandong University) for kindly providing the *MiR396a* and *MIM396* overexpression lines, and Feng Yu for kindly providing *PE3308* and *PE3449* vectors (School of Life Science, Hunan University). This work was supported by grants from National Natural Science Foundation of China (31571499, 31872663, 31961133001) and the strategic priority research programme of the Chinese Academy of Sciences (XDB27010102).

Author contributions

Y.L., H.L., L.Z. and H.W. conceived and designed the experiments. Y.L., H.L. supervised this project. L.Z., H.W. and A.W. performed most of the experiments. Y.Z. screened the SOD7 interaction protein GIF1 and did some phenotype analysis. Z.L. analysed outer integument development. L.Z., H.W., A.W., Y.L., H.L. and X.S. analysed and discussed the data. L.Z. wrote the paper. Y.L., H.L., X.S., H.W. and A.W. revised paper.

Competing interests

The authors declare no competing interests.

Additional information

Extended data is available for this paper at https://doi.org/10.1038/s41477-023-01475-0.

Supplementary information The online version contains supplementary material available at https://doi.org/10.1038/s41477-023-01475-0.

Correspondence and requests for materials should be addressed to Hong-Qing Ling, Xian-Jun Song or Yunhai Li.

Peer review information *Nature Plants* thanks Jeeyon Jeong, Jeong-Hoe Kim and the other, anonymous, reviewer(s) for their contribution to the peer review of this work.

https://doi.org/10.1038/s41477-023-01475-0

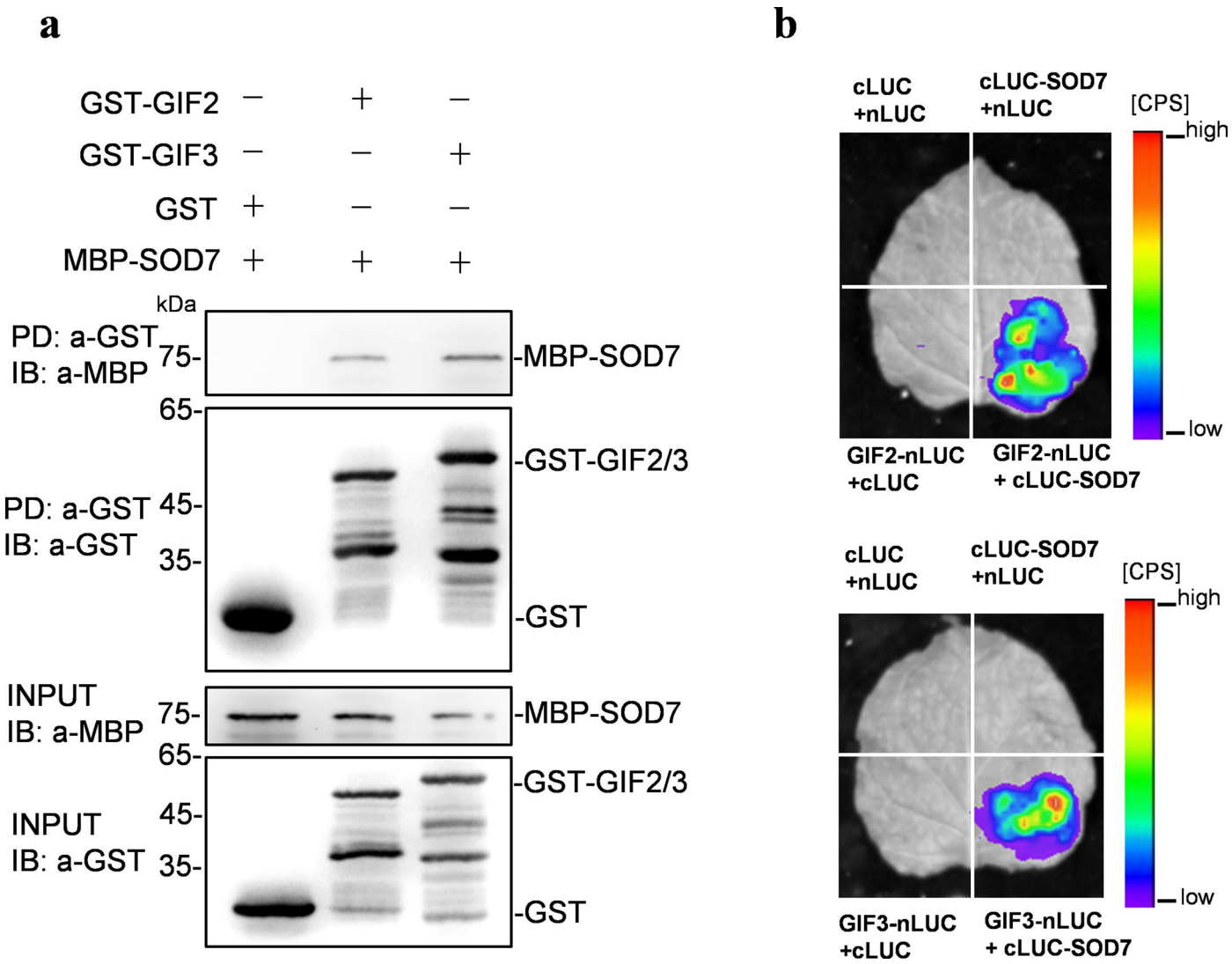

Extended Data Fig. 1 | SOD7 interacts with GIF2/3 in vitro and in vivo. a, SOD7 interacts with GIF2/3 in pull-down assays. MBP–SOD7 was pulled down by GST–GIF2/3 immobilized on GST beads and analysed by immunoblotting with an anti-GST or anti-MBP antibody. **b**, The interaction between SOD7 and GIF2/3 was detected by split luciferase complementation assays. *N. benthamiana* leaves were co-infiltrated with the *Agrobacterium* GV3101 containing different plasmids combinations for 48 h and then images were determined by a CCD camera. The pseudocolor scale bar was used to indicate the range of luminescence intensity. All experiments were repeated independently twice with similar results.

https://doi.org/10.1038/s41477-023-01475-0

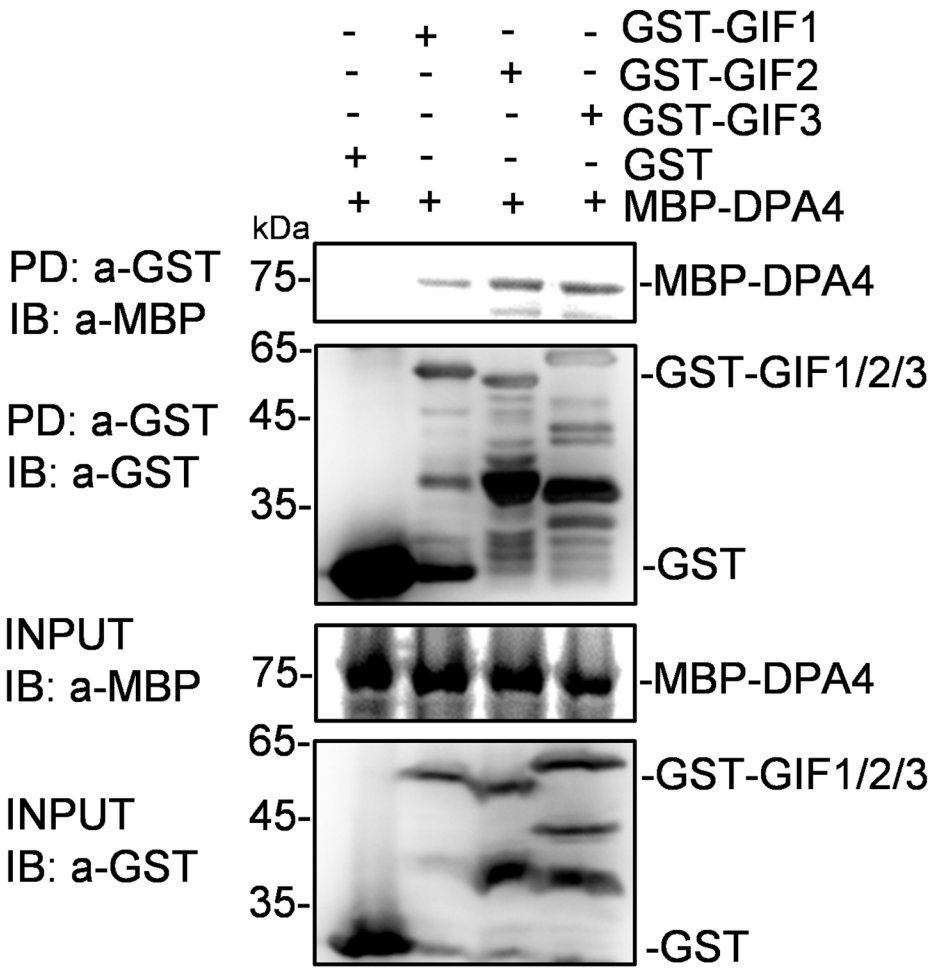

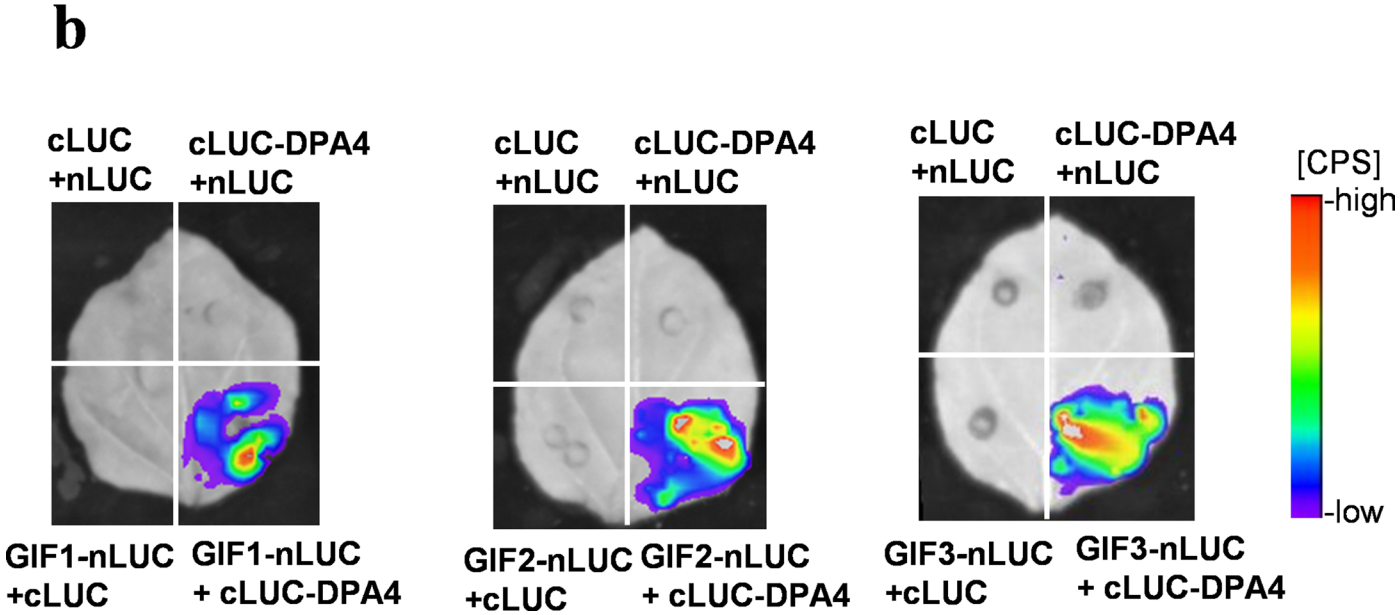

Extended Data Fig. 2 | DPA4 interacts with GIF1/2/3 in vitro and in vivo. a, DPA4 interacts with GIF12/3 in pull-down assays. MBP–DPA4 was pulled down by GST–GIF1/2/3 immobilized on GST beads and analysed by immunoblotting with an anti-GST or anti-MBP antibody. **b**, The interaction between DPA4 and GIF1/2/3 was detected by split luciferase complementation assays. *N. benthamiana* leaves were co-infiltrated with the *Agrobacterium* GV3101 containing different plasmids combinations for 48 h and then images were determined by a CCD camera. The pseudocolor scale bar was used to indicate the range of luminescence intensity. All experiments were repeated independently twice with similar results.

https://doi.org/10.1038/s41477-023-01475-0

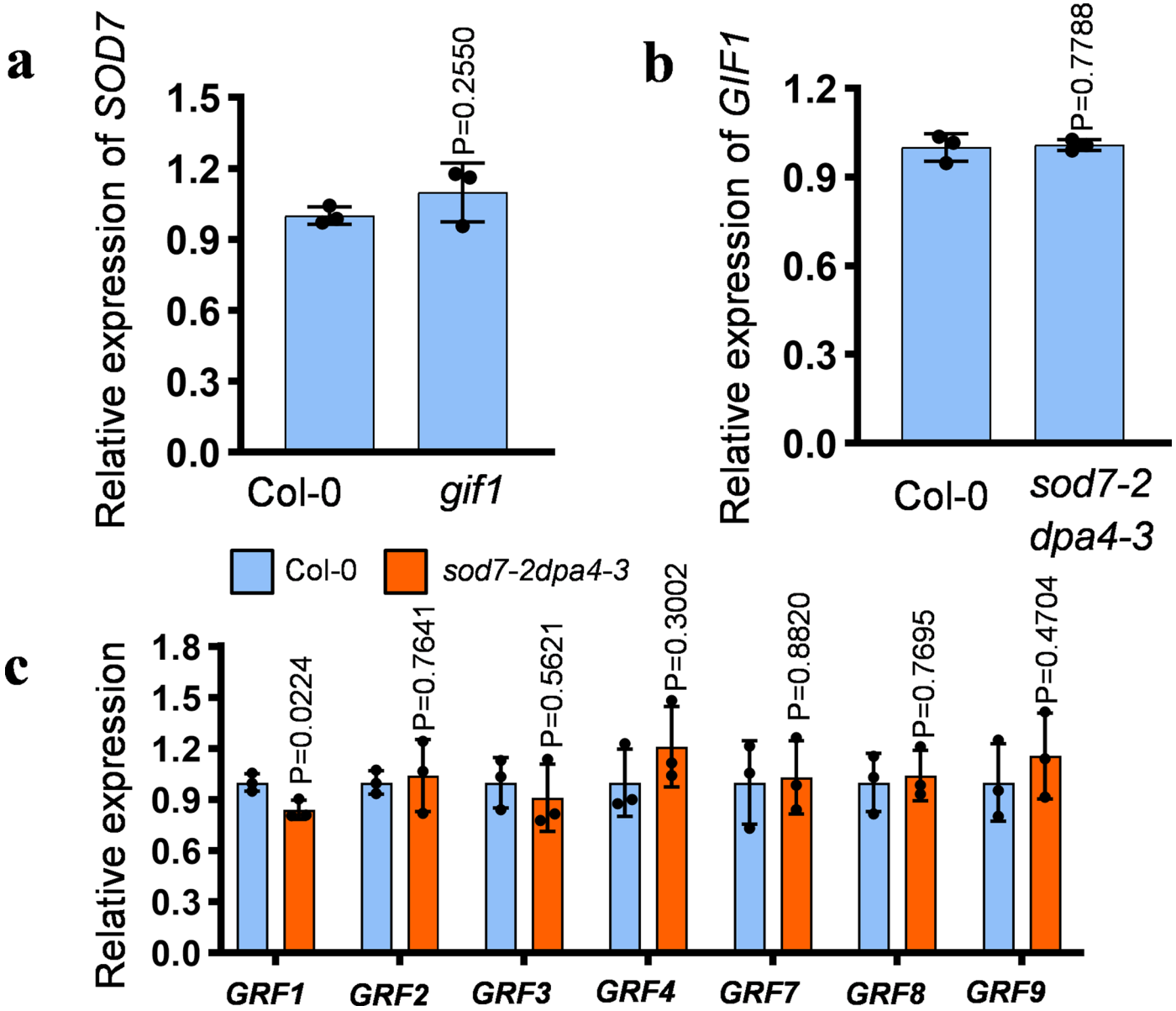

Extended Data Fig. 3 | The relative expression analysis. a. The relative expression level of *SOD7* in flowers of Col-0 and *gif1*. **b.** The relative expression level of GIF1 in flowers of Col-0 and *sod7-2 dpa4-3*. **c.** GRFs expression levels in flowers of Col-0 and *sod7-2 dpa4-3*. All the data were shown as mean ± SD with three biological repeats. Two-tailed unpaired t-test for **a** and **b**, Multiple t-test followed two-tailed unpaired t-test per row for **c**.

https://doi.org/10.1038/s41477-023-01475-0

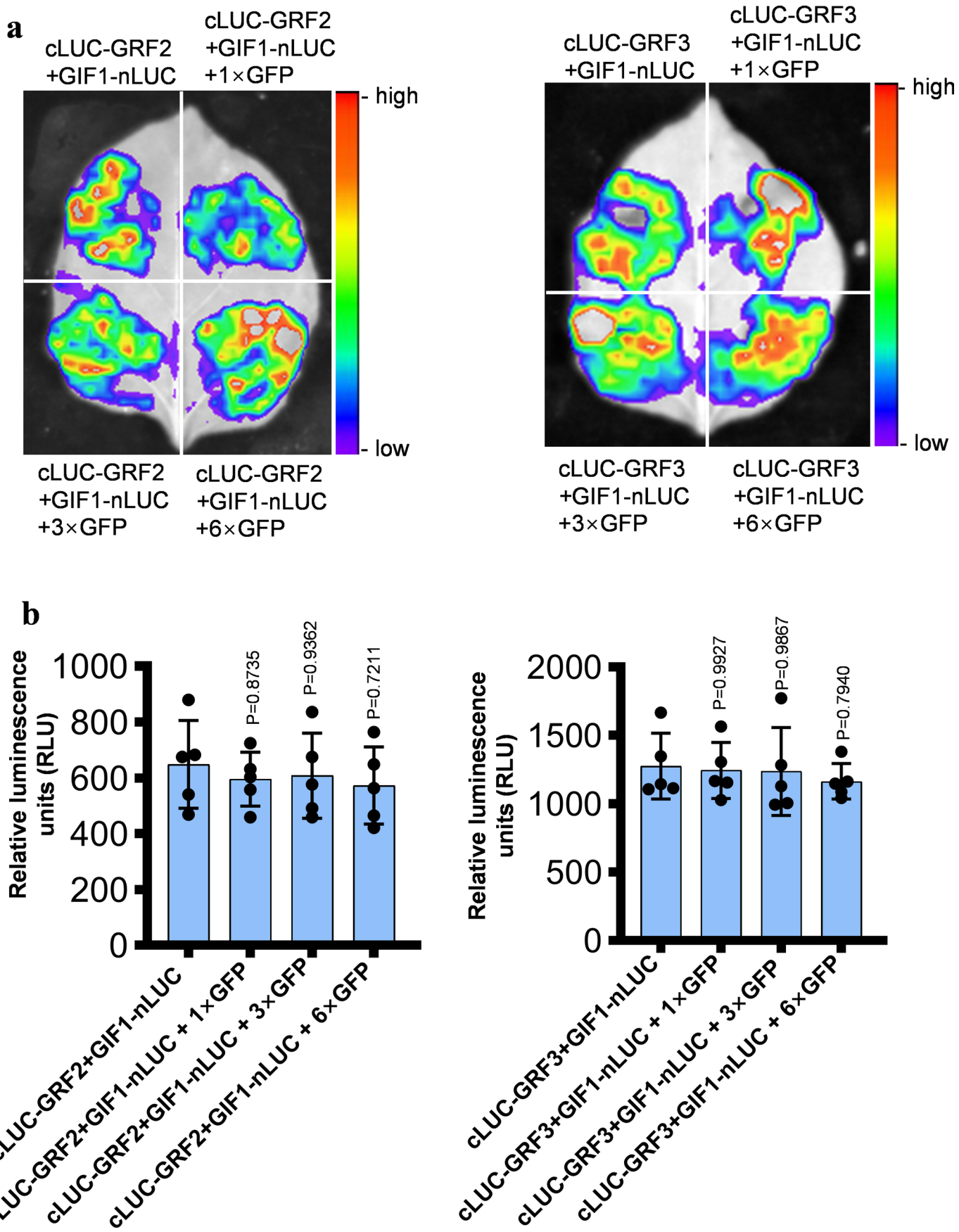

Extended Data Fig. 4 | The interactions between GIF1 and GRF2/3 were not affected by GFP protein. a. The GFP did not affect the interaction between GIF1 and GRF2/GRF3 detected by split luciferase complementation assays. The leaves of *N. benthamiana* were co-infiltrated with the *Agrobacterium* GV3101 containing combinations as indicated. The pseudocolor scale bar was used to indicate the range of luminescence intensity. **b**. Quantification of LUC signals from **a**. Values represent mean ± SD (n = 5 biologically independent samples). One-way ANOVA (Dunnett's multiple comparisons test, P = 0.05) was used for statistical analysis.

https://doi.org/10.1038/s41477-023-01475-0

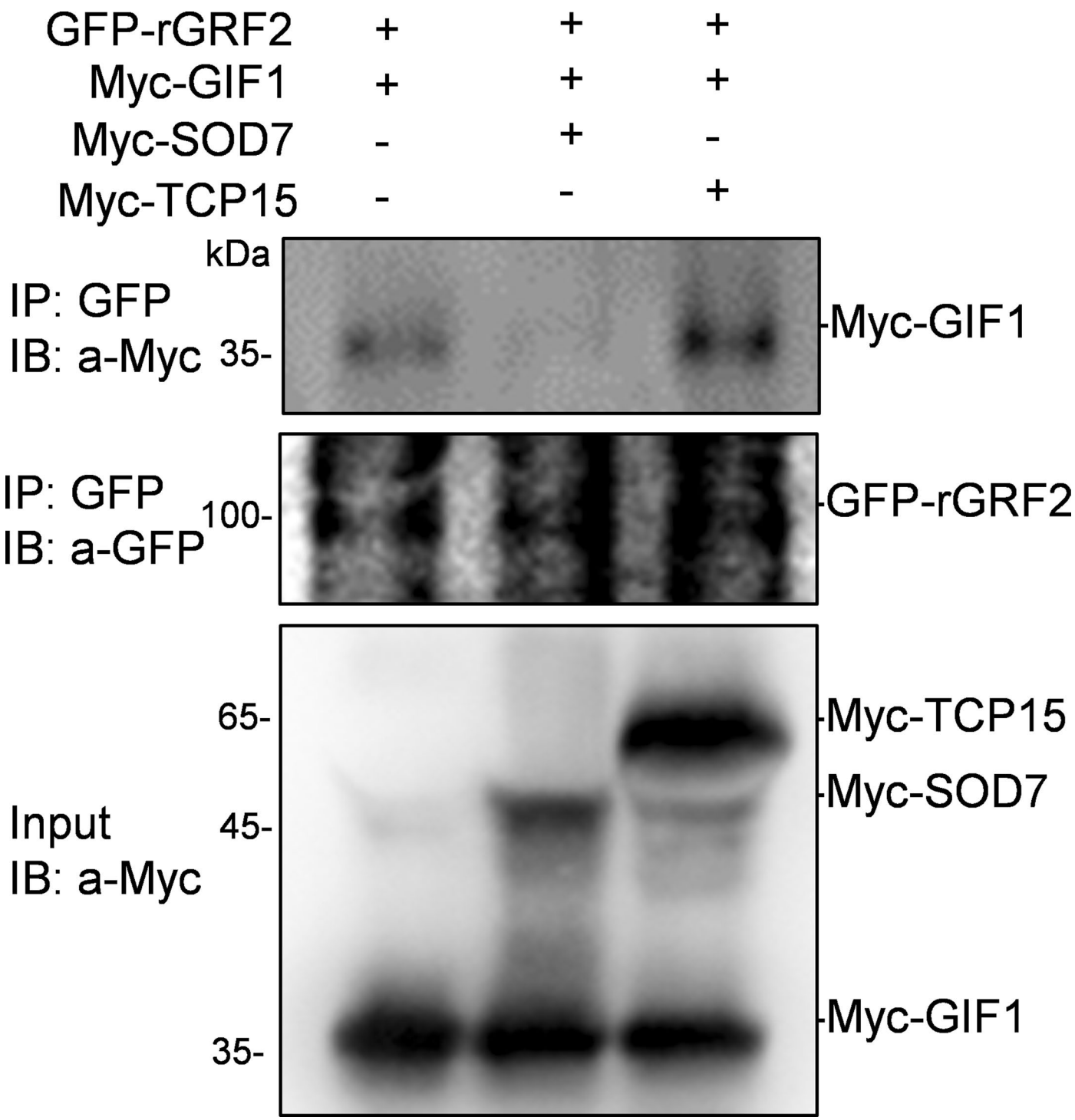

Extended Data Fig. 5 | SOD7 competes suppressing the interaction between GIF1 and GRF2. The combinations of different plasmids as indicated were overexpressed in *N. benthamiana* leaves. The *N. benthamiana* leaves were grown for another 3 days before the total proteins were extracted. The proteins were immunoprecipitated with GFP–Trap-A beads, and detected with anti-Myc and anti-GFP antibodies, respectively. The experiments were repeated independently twice with similar results.

https://doi.org/10.1038/s41477-023-01475-0

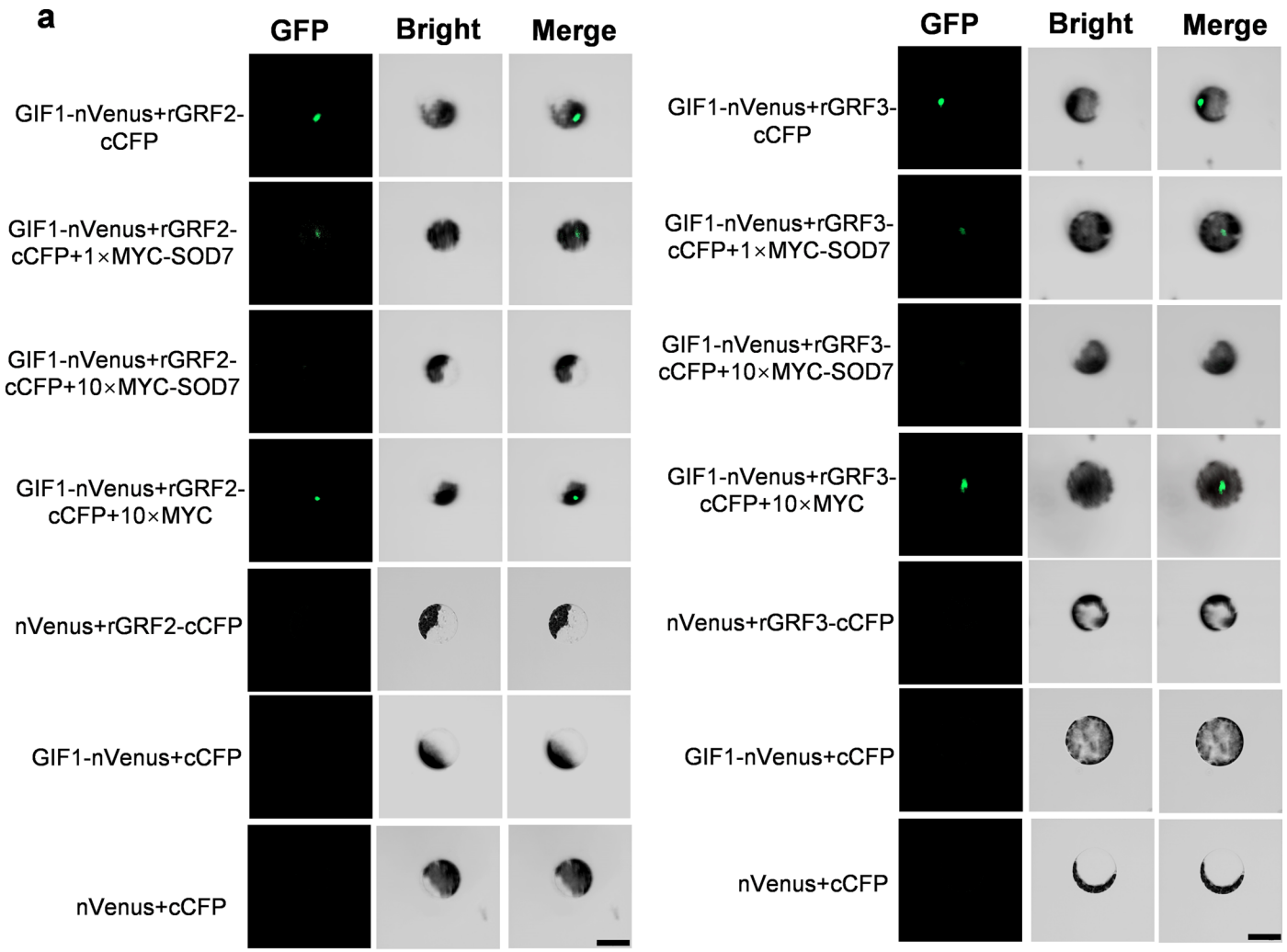

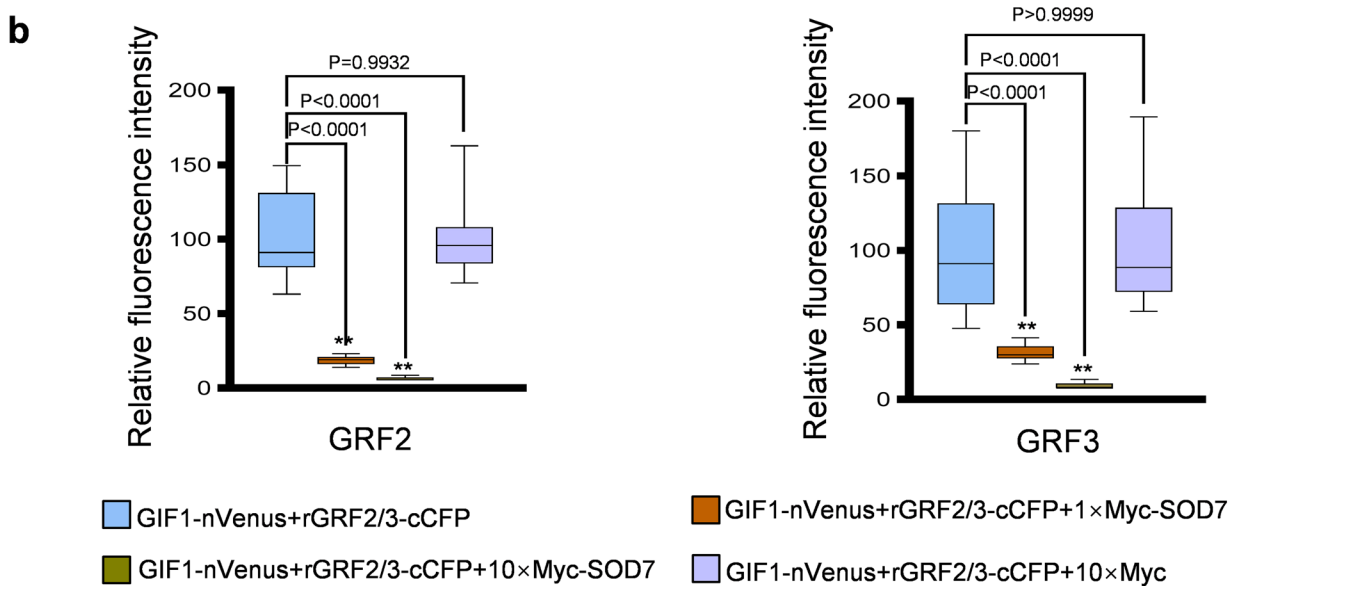

Extended Data Fig. 6 | SOD7 competes suppressing the interaction between GIF1 and GRF2/3 in *sod7-2 dpa4-3* protoplast. a. GIF1–nVenus and rGRF2/3–cCFP, plus different concentration of Myc–SOD7 as indicated were co-transformed into *sod7-2 dpa4-3* protoplasts. the 10xMyc was used as a negative control. bar = 40 μm. **b**. Quantification of GFP signals from **a**. Values represent mean ± SD (n = 16 protoplasts for GRF2 and n = 20 for GRF3). Asterisk indicates significant difference, **P < 0.01 compared with GIF1–nVenus+rGRF2/3–cCFP samples, and the corresponding GIF1–nVenus+rGRF2/3–cCFP set as 100. One-way ANOVA (Dunnett's multiple comparisons test) was used for statistical analysis. In the box plots for **b**, the centre lines are the median and the edges of the box are the lower and upper quartiles. Whiskers extend to the lowest and highest data points.

https://doi.org/10.1038/s41477-023-01475-0

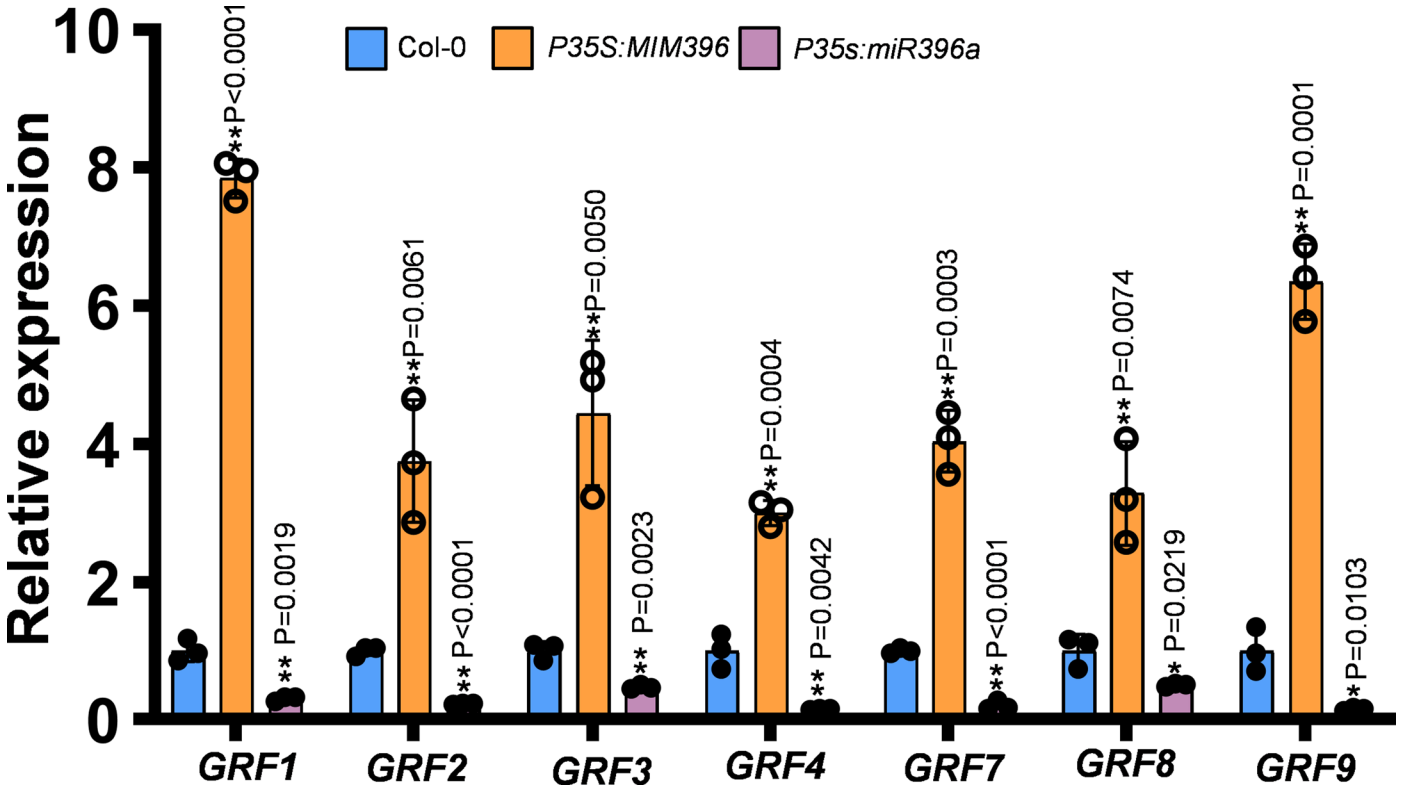

Extended Data Fig. 7 | qRT-PCR analysis of the expression level of *GRFs* in 7d seedlings of Col-0, *35Spro:MIM396* and *35Spro:miR396a*. The *ACTIN2* gene was used as an internal control. Data are shown as means ± SD (n = 3 biologically independent samples). * $p < 0.05$, ** $p < 0.01$ compared with Col-0 and the corresponding Col-0 data set as 1(Multiple t-test followed two-tailed unpaired t-test per row).

https://doi.org/10.1038/s41477-023-01475-0

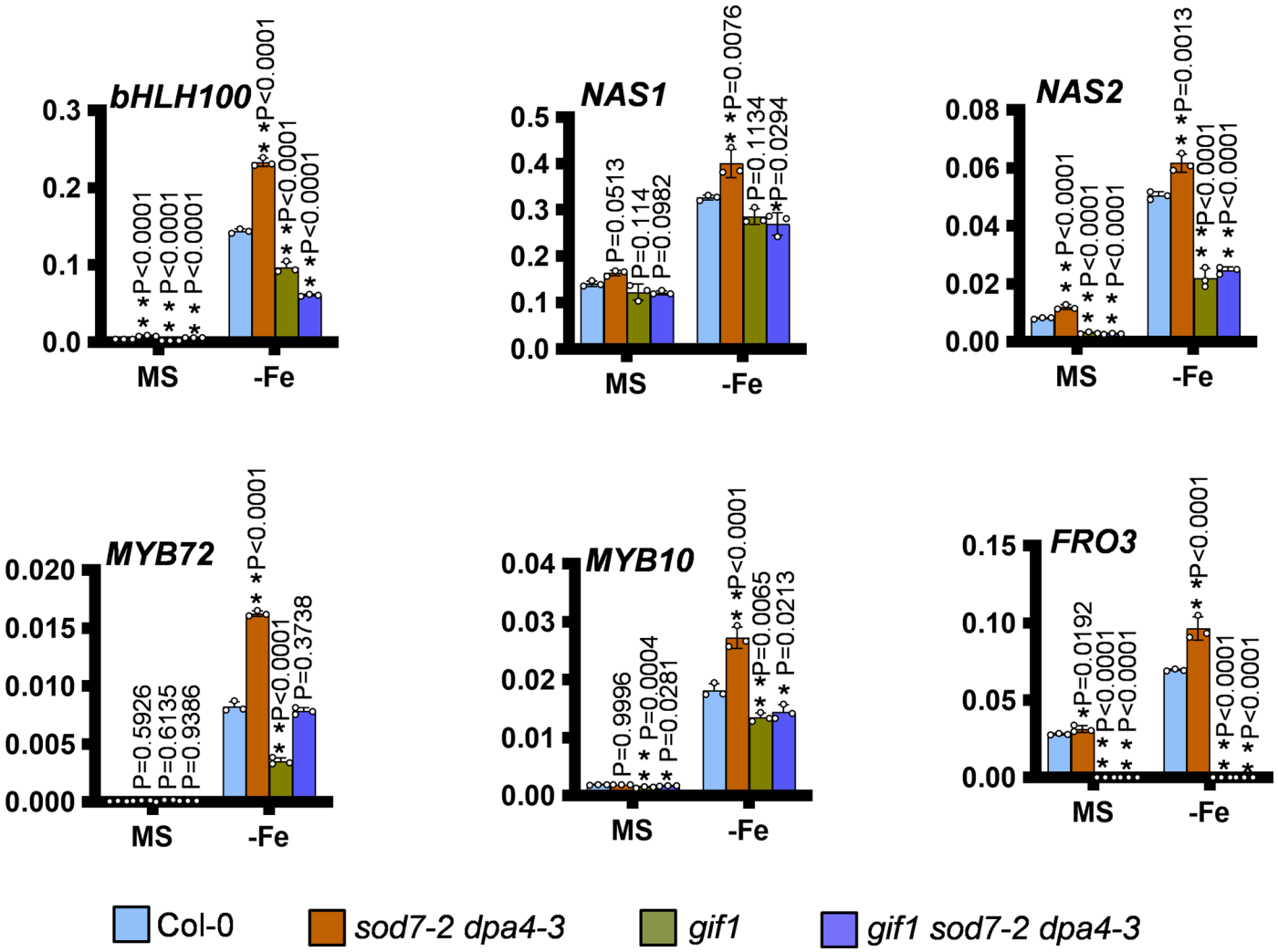

Extended Data Fig. 8 | The relative expression level of –Fe-responsive genes in roots of Col-0 and mutants grown on MS medium with or without 100uM Fe. Data represent mean ± SD, n = 3 for three biological replicates. Asterisk indicates significant difference, *P < 0.05 and **P < 0.01 compared with the wild type. One-way ANOVA (Dunnett's multiple comparisons test) was used for statistical analysis.

https://doi.org/10.1038/s41477-023-01475-0

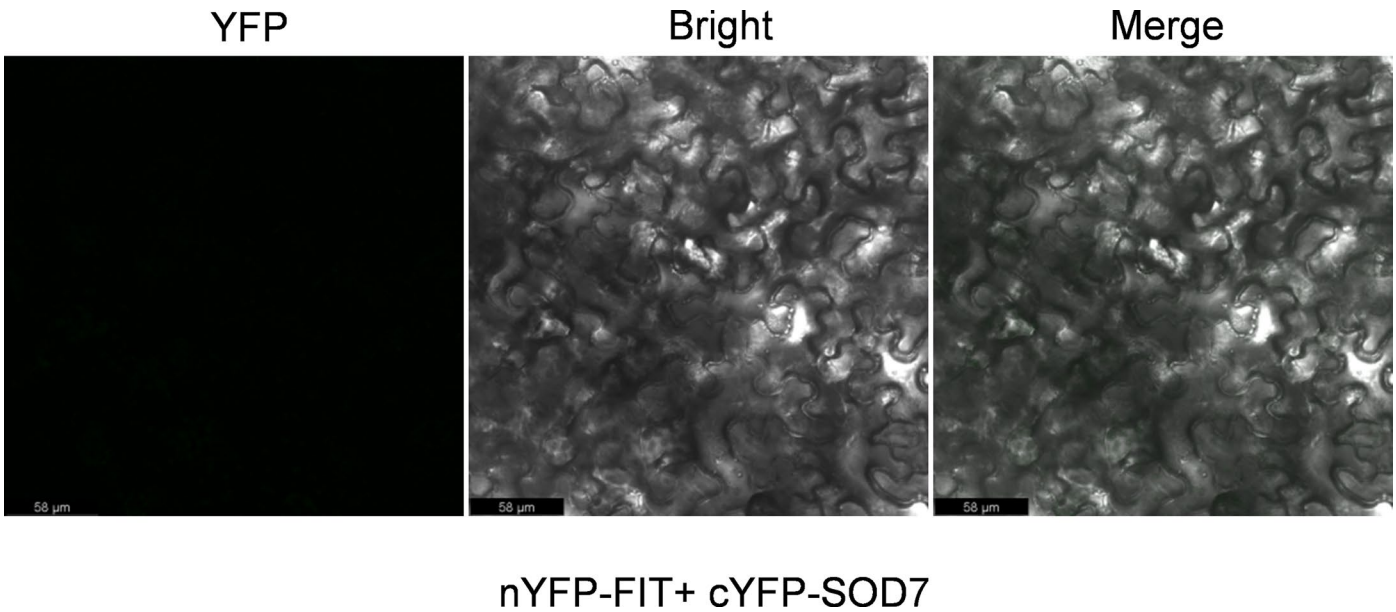

Extended Data Fig. 9 | SOD7 did not interact with FIT in BiFC assays. The experiment was repeated independently three times with similar results.

https://doi.org/10.1038/s41477-023-01475-0

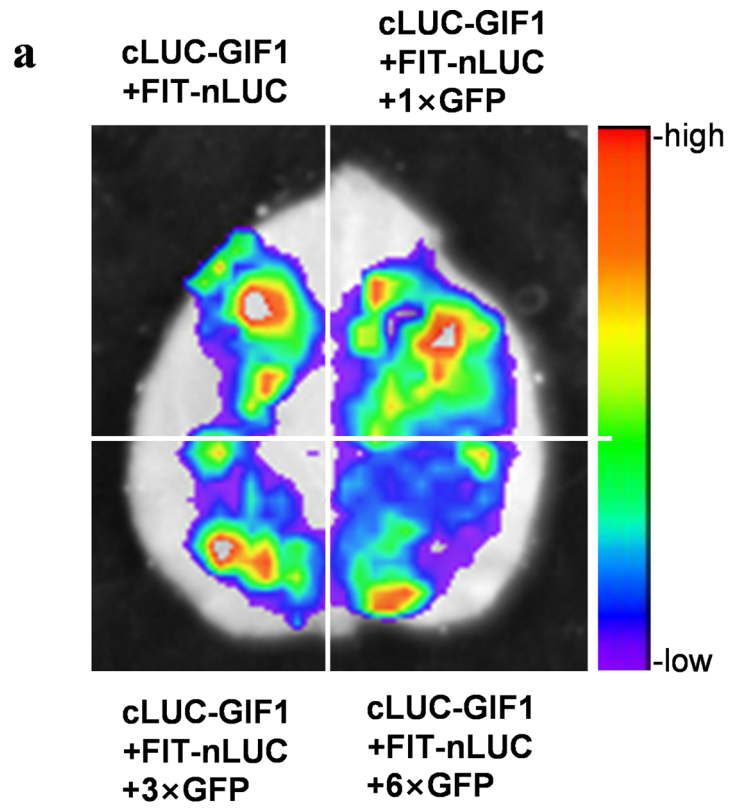

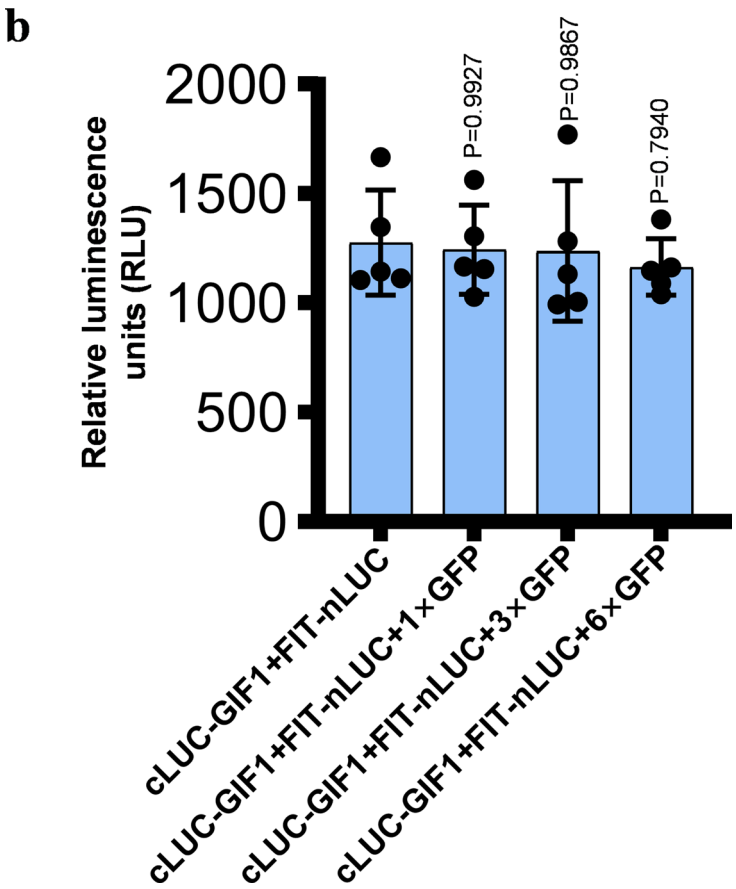

Extended Data Fig. 10 | See next page for caption.

https://doi.org/10.1038/s41477-023-01475-0

Extended Data Fig. 10 | The interaction between GIF1 and FIT was not affected by GFP protein. a. The GFP did not affect the interaction between GIF1 and FIT detected by split luciferase complementation assays. The leaves of *N. benthamiana* were co-infiltrated with the *Agrobacterium* GV3101 containing combinations as indicated. The pseudocolor scale bar was used to indicate the range of luminescence intensity. **b**. Quantification of LUC signals from **a**. Values represent mean ± SD (n = 5 biologically independent samples). One-way ANOVA ((Dunnett's multiple comparisons test, p = 0.05) was used for statistical analysis, cLUC-GIF1 + FIT-nLUC was used as control.

nature portfolio

Corresponding author(s): Yunhai Li, Xian-Jun Song, Hong-Qing Ling

Last updated by author(s): Jun 27, 2023

Reporting Summary

Nature Portfolio wishes to improve the reproducibility of the work that we publish. This form provides structure for consistency and transparency in reporting. For further information on Nature Portfolio policies, see our Editorial Policies and the Editorial Policy Checklist.

Statistics

For all statistical analyses, confirm that the following items are present in the figure legend, table legend, main text, or Methods section.

n/a	Confirmed	
☐	☒	The exact sample size (*n*) for each experimental group/condition, given as a discrete number and unit of measurement
☐	☒	A statement on whether measurements were taken from distinct samples or whether the same sample was measured repeatedly
☐	☒	The statistical test(s) used AND whether they are one- or two-sided *Only common tests should be described solely by name; describe more complex techniques in the Methods section.*
☒	☐	A description of all covariates tested
☒	☐	A description of any assumptions or corrections, such as tests of normality and adjustment for multiple comparisons
☐	☒	A full description of the statistical parameters including central tendency (e.g. means) or other basic estimates (e.g. regression coefficient) AND variation (e.g. standard deviation) or associated estimates of uncertainty (e.g. confidence intervals)
☐	☒	For null hypothesis testing, the test statistic (e.g. *F*, *t*, *r*) with confidence intervals, effect sizes, degrees of freedom and *P* value noted *Give P values as exact values whenever suitable.*
☒	☐	For Bayesian analysis, information on the choice of priors and Markov chain Monte Carlo settings
☒	☐	For hierarchical and complex designs, identification of the appropriate level for tests and full reporting of outcomes
☒	☐	Estimates of effect sizes (e.g. Cohen's *d*, Pearson's *r*), indicating how they were calculated

Our web collection on statistics for biologists contains articles on many of the points above.

Software and code

Policy information about availability of computer code

Data collection	The organ and seed size were photographed using a Leica S8APO or Leica DM2500 microscope. Samples for elements were digested by ETHOSl Microwave Digestion System (Milestone, Italy) and determined by ICP-OES, model 5300DV, Perkin Elmer, Inc., USA. Luciferase complementation images were taken on NightOWL II LB983. Western blot images were scanned using Tanon-4500. Luminescence recording was detected in GLOMAX 96 microplate luminometer. Bimolecular fluorescence images were collected on Leica SP8 Confocal microscope system.
Data analysis	Image⊟(Version 1.53); Adobe Photoshop 2021(version: 2.0); Zen Black (Zeiss); GraphPad Prisms (GraphPad Software).

For manuscripts utilizing custom algorithms or software that are central to the research but not yet described in published literature, software must be made available to editors and reviewers. We strongly encourage code deposition in a community repository (e.g. GitHub). See the Nature Portfolio guidelines for submitting code & software for further information.

Data

Policy information about availability of data

All manuscripts must include a data availability statement. This statement should provide the following information, where applicable:

- Accession codes, unique identifiers, or web links for publicly available datasets
- A description of any restrictions on data availability
- For clinical datasets or third party data, please ensure that the statement adheres to our policy

All materials in this study are available from the corresponding author upon request. The authors declare that all data supporting the findings of this study are available within the article and its Supplementary Information files. Arabidopsis reference genome (TAIR10) was used in this study. The primers used in this study are provided as Supplementary Table 2. Source data are provided with this paper.

Research involving human participants, their data, or biological material

Policy information about studies with human participants or human data. See also policy information about sex, gender (identity/presentation), and sexual orientation and race, ethnicity and racism.

Reporting on sex and gender	*Use the terms sex (biological attribute) and gender (shaped by social and cultural circumstances) carefully in order to avoid confusing both terms. Indicate if findings apply to only one sex or gender; describe whether sex and gender were considered in study design; whether sex and/or gender was determined based on self-reporting or assigned and methods used.* *Provide in the source data disaggregated sex and gender data, where this information has been collected, and if consent has been obtained for sharing of individual-level data; provide overall numbers in this Reporting Summary. Please state if this information has not been collected.* *Report sex- and gender-based analyses where performed, justify reasons for lack of sex- and gender-based analysis.*
Reporting on race, ethnicity, or other socially relevant groupings	*Please specify the socially constructed or socially relevant categorization variable(s) used in your manuscript and explain why they were used. Please note that such variables should not be used as proxies for other socially constructed/relevant variables (for example, race or ethnicity should not be used as a proxy for socioeconomic status).* *Provide clear definitions of the relevant terms used, how they were provided (by the participants/respondents, the researchers, or third parties), and the method(s) used to classify people into the different categories (e.g. self-report, census or administrative data, social media data, etc.)* *Please provide details about how you controlled for confounding variables in your analyses.*
Population characteristics	*Describe the covariate-relevant population characteristics of the human research participants (e.g. age, genotypic information, past and current diagnosis and treatment categories). If you filled out the behavioural & social sciences study design questions and have nothing to add here, write "See above."*
Recruitment	*Describe how participants were recruited. Outline any potential self-selection bias or other biases that may be present and how these are likely to impact results.*
Ethics oversight	*Identify the organization(s) that approved the study protocol.*

Note that full information on the approval of the study protocol must also be provided in the manuscript.

Field-specific reporting

Please select the one below that is the best fit for your research. If you are not sure, read the appropriate sections before making your selection.

☒ Life sciences ☐ Behavioural & social sciences ☐ Ecological, evolutionary & environmental sciences

For a reference copy of the document with all sections, see nature.com/documents/nr-reporting-summary-flat.pdf

Life sciences study design

All studies must disclose on these points even when the disclosure is negative.

Sample size	No statistical approach was used to predetermine sample size. Sample sizes were selected empirically from previous experimental experience with similar assays, and/or from sizes generally employed in the field
Data exclusions	No data was excluded from analysis in the experiments.
Replication	All Experiments were repeated as indicated and the data were reproducible using the same experimental conditions.
Randomization	All the samples were collected randomly.
Blinding	All the experiments were performed with no prior expected results, and therefore blinding was not existed.

Reporting for specific materials, systems and methods

We require information from authors about some types of materials, experimental systems and methods used in many studies. Here, indicate whether each material, system or method listed is relevant to your study. If you are not sure if a list item applies to your research, read the appropriate section before selecting a response.

Materials & experimental systems

n/a	Involved in the study
☐	☒ Antibodies
☒	☐ Eukaryotic cell lines
☒	☐ Palaeontology and archaeology
☒	☐ Animals and other organisms
☒	☐ Clinical data
☒	☐ Dual use research of concern
☐	☒ Plants

Methods

n/a	Involved in the study
☒	☐ ChIP-seq
☒	☐ Flow cytometry
☒	☐ MRI-based neuroimaging

Antibodies

Antibodies used

anti-GST (1:5000, Abmart, M20007), anti-MBP antibody (NEB E8032, 1: 10, 000), anti-GFP (Abmart M20004, 1: 5,000) and anti-Myc (Abmart M20002, 1: 5,000) were purchased from Abmart (Shanghai, China)., anti-FIT (1:1000) and anti-IRTl(l:1000) were produced from the lab. GFP-Trap'" agarose (#gta-20, ChromoTek Germany), anti-Myc-Tag (agarose con□ugated, M20012, Abmart, China), Glutath1one SepharoseTM 4B (#45-000-139,GE Healthcare, USA)), amylase resin(#E8021, New England Biolabs) and one step western kit HRP {#CW2030, Cwbiotech, China)

Validation

Information of anti-GST validation can be found at website: http://www.ab-mart.corn.cn/page.aspx? node=60&id=967
Information of anti-MBP validation can be found at website: https://www.neb.cn/products/e8032-anti-mbp-monoclonal-antibody
Information of anti-GFP validation can be found at website: http://www.ab-mart.corn.cn/page.aspx?node=60&id=971
Information of anti-Myc validation can be found at website: http://www.ab-mart.corn.cn/page.aspx?node=60&id=962
Information of GFP-Trap agarose can be found at website: https://www.chromotek.com/products/detail/product-detail/gfp-trap-agarose/
Information of anti-Myc-Tag validation can be found at website: http://www.ab-mart.corn.cn/page.aspx?node=%2061%20&id=%20961
Information of amylase resin validation can be found at website: https://www.neb.com/products/e8021-amylose-resin#Product% 20
Information of one step western kit HRP validation can be found at website: https://www.cwbiotech.com/goods/index/id/10294
Information of Glutathione SepharoseTM 4B validation can be found at website: https://www.fishersci.com/shop/products/ge-healthcare-glutathione-sepharose-4b-media-3/45000139